REPORT NO. DOT-TSC-212-72-1.

FUNCTIONAL ERROR ANALYSIS AND MODELING FOR ATC SYSTEMS CONCEPTS EVALUATION.

William C. Hoffman
Walter M. Hollister
Robert W. Simpson
Aerospace Systems Inc.
One Vine Brook Park
Burlington, MA.   01803

MAY 1972

FINAL REPORT

Prepared for
DEPARTMENT OF TRANSPORTATION.
OFFICE OF THE SECRETARY
Office of Systems Engineering
Washington, D.C.   20590

1. Report No. DOT-TSC-212-72-1	2. Government Accession No.	3. Recipient's Catolog
4. Title and Subtitle Functional Error Analysis and Modeling for ATC System Concepts Evaluation		5. Report Date May 1972
		6. Performing Organization Code
7. Author(s) William C. Hoffman, Walter M. Hollister (MIT), Robert W. Simpson (MIT)		8. Performing Organization Report No. ASI-TR-72-9
9. Performing Organization Name and Address Aerospace Systems, Inc. One Vine Brook Park Burlington, Massachusetts 01803		10. Work Unit No.
		11. Contract or Grant No. DOT-TSC-212
12. Sponsoring Agency Name and Address Transportation Systems Center 55 Broadway Cambridge, Massachusetts 02142		13. Type of Report and Period Covered Final Technical Report May 1971 through May 1972
		14. Sponsoring Agency Code

15. Supplementary Notes

16. Abstract

A functional error analysis and modeling study of the air traffic control (ATC) system is described. The work was performed to support the ATC system concepts evaluation program of the Transportation Systems Center (TSC), which will be conducted on their Multi-Modal Transportation System Simulation. The dominant functional error sources in the ATC system are identified and models of these errors are developed for implementation in the TSC simulation. The models are constructed to be as realistic as possible without placing excessive computational requirements on their realization. The models were developed in four categories: target dynamics, air data system, navigation systems and surveillance systems. The simulation wind model was also improved. The performance of the altitude, airspeed and heading command loops in the target dynamics model were numerically verified by digital computer simulation.

17. Key Words Air traffic control, error analysis, error models, simulation, target dynamics, air data system, navigation systems, surveillance systems.	18. Distribution Statement DOCUMENT IS AVAILABLE TO THE PUBLIC THROUGH THE NATIONAL TECHNICAL INFORMATION SERVICE, SPRINGFIELD, VIRGINIA 22151.		
19. Security Classif. (of this report) Unclassified	20. Security Classif. (of this page) Unclassified	21. No. of Pages 98	22. Price

PREFACE

This report was prepared by Aerospace Systems, Inc. (ASI), Burlington, Massachusetts, for the Department of Transportation under Contract No. DOT-TSC-212. The program was sponsored by the Transportation Systems Center (TSC), Cambridge, Massachusetts. Dr. Robert J. Hynes of the Technology Directorate served as Technical Monitor on the contract.

This document is the final scientific report which presents the results of research performed during the contract period May 1971 through May 1972. The effort was directed by Mr. John Zvara, President and Technical Director of ASI. Mr. William C. Hoffman served as Principal Investigator. Dr. Robert W. Simpson, Head of the Flight Transportation Laboratory, and Dr. Walter M. Hollister, both in the Department of Aeronautics and Astronautics at the Massachusetts Institute of Technology, contributed to the study as Technical Consultants.

TABLE OF CONTENTS

LIST OF ILLUSTRATIONS

NOMENCLATURE[*]

d	=	DME distance corrected for altitude; nm [RNAV]
	=	cross-track distance from desired track; nm [target dynamics]
d'	=	indicated distance from waypoint to aircraft; nm
d_w	=	distance from VOR/DME station to waypoint; nm
$e_{(\ )}$	=	$(\ )_c - (\ )_I$ = difference between commanded and indicated values of appropriate variable
g	=	gravitational force per unit mass; 32.2 ft/sec^2
h	=	altitude above coordinate origin; ft
h_a	=	measured aircraft altitude; ft
h_s	=	VOR/DME station altitude; ft
m,n	=	radar range and azimuth bin indices [ground surveillance]
P_t, P_s	=	total and static pressure measured by air data system; lb/ft^2
t	=	time; sec
w_D, w_V	=	white noise for DME and VOR errors; nm, deg
x,y	=	horizontal position coordinates east and north, respectively, of origin; nm
x_p, y_p	=	predicted aircraft position coordinates, east and north; nm [radar tracking]

[*]Where nomenclature may be confusing, the appropriate model is indicated in brackets.

x_r, y_r	=	surveillance antenna coordinates, east and north of origin; nm
A_x, A_y	=	longitudinal and lateral aerodynamic force per unit mass; kt/min, ft/sec^2
D	=	horizontal distance between VOR/DME$_1$ and DME$_2$ stations; nm [DME/DME RNAV]
F	=	flight plan information
K_1, K_2	=	course tracking gains; deg/nm, nm/deg [target dynamics]
$K_{\dot{h}}, K_M, K_V$	=	indicator scale factor errors [air data system]
M	=	Mach number.
$N[m, \sigma]$	=	Gaussian random number with mean m and standard deviation σ
P	=	general aircraft position vector
R	=	slant range to aircraft; nm
R_r	=	measured slant range from radar to aircraft; nm
R_D	=	indicated slant range from DME station to aircraft; nm
T	=	radar scan period; sec .
T_D	=	DME error correlation time; sec
V_a	=	true airspeed of aircraft; kt
V_g	=	true groundspeed of aircraft; kt
V_{CAS}	=	calibrated airspeed; kt

V_{IAS} = indicated airspeed; kt

V_S = local speed of sound; kt

α = weighting parameter for aircraft position update [radar tracking]

= indicated bearing of aircraft position from VOR/DME_1 station; deg [DME/DME RNAV]

α_0 = true bearing of DME_2 station from VOR/DME_1 station; deg [DME/DME RNAV]

β = weighting parameter for aircraft velocity update [radar tracking]

γ = elevation of line-of-sight from radar to aircraft above horizontal; deg

$\delta(t)$ = Dirac delta function

$\Delta R, \Delta\theta$ = radar range and azimuth bin sizes; nm, deg [ground surveillance]

$\varepsilon_h, \varepsilon_{\dot{h}}$ = instrument errors in altimeter and vertical speed indicator; ft, ft/min [air data system]

$\varepsilon_A, \varepsilon_R$ = radar azimuth and range errors; deg, nm [ground surveillance]

ε_c = VOR course roughness error; deg

ε_D = DME total error; nm

$\varepsilon_I, \varepsilon_S$ = DME bias errors in interrogator and station transponder; nm

$\varepsilon_R, \varepsilon_T$ = VOR bias errors in receiver and transmitter; deg

ε_V = VOR total error; deg

ϵ_ψ	=	instrument error in heading indicator; deg [air data system]
ζ_n	=	desired tracking loop damping ratio [target dynamics]
η	=	+ 1 or − 1 to indicate $\alpha < \alpha_0$ or $\alpha > \alpha_0$ [DME/DME/RNAV]
θ	=	true bearing from station to aircraft; deg
θ'	=	bearing waypoint to aircraft; deg [RNAV]
θ_r	=	measured azimuth of aircraft; deg [surveillance]
θ_w	=	indicated bearing from waypoint to aircraft; deg [RNAV]
	=	wind direction; deg [target dynamics]
θ_M	=	magnetic variation at VOR/DME station; deg
θ_V	=	indicated bearing from VOR/DME station to aircraft; deg
ρ, ρ_0	=	local and sea level values of atmospheric density; slug/ft^3
σ	=	maximum bank angle; deg [target dynamics]
σ_A, σ_R	=	standard deviations of ϵ_A, ϵ_R; deg, nm [ground surveillance]
$\sigma_c, \sigma_R, \sigma_T$	=	standard deviations of $\epsilon_c, \epsilon_R, \epsilon_T$; deg [VOR/DME]
$\sigma_D, \sigma_I, \sigma_S$	=	standard deviations of $\epsilon_D, \epsilon_I, \epsilon_S$; nm [VOR/DME]
σ_ψ	=	standard deviation of ϵ_ψ; deg [air data system]
$\tau_{(\ )}$	=	first order time lag in ( ); sec
ϕ	=	bank angle; deg

χ $=$ ground track angle; deg

ψ $=$ heading angle; deg

ω $=$ standard rate of turn; deg/sec [target dynamics]

ω_c $=$ VOR course roughness frequency; rad/sec/kt

ω_n $=$ desired natural tracking frequency; rad/sec [target dynamics]

Ω $=$ scan rate of radar; rpm [surveillance system]

$\mathcal{E}(\ )$ $=$ expected value of indicated quantity

Subscripts

$(\ )_a$ $=$ value at aircraft location

$(\ )_i$ $=$ value of indicated quantity on radar scan i [surveillance system]

$(\ )_{max}$ $=$ maximum value of indicated quantity

$(\ )_r$ $=$ value at radar site

$(\ )_s$ $=$ value at VOR/DME station

$(\ )_I$ $=$ indicated value of measured variable [air data system]

Superscripts

$(\ )^c$ $=$ sector controller

$(\ )^t$ $=$ target aircraft

Miscellaneous

$\widehat{(\ )}$ = estimated value of ( )

$\dot{(\ )}$ = derivative with respect to time

$\underline{(\ )}$ = vector quantity

SECTION I

INTRODUCTION

The Department of Transportation Transportation Systems Center (DOT TSC) is developing a Multi-Modal Transportation System Simulation with real-time capability for simulating the command and control functions related to various transportation systems (Ref. 1). The first phase of this effort is producing an Advanced Air Traffic Control (ATC) Simulation Laboratory to define and evaluate the most effective role of the controller in advanced generation ATC systems, and to assess quantitatively various control strategies and automated techniques in these systems. The objective is to provide and exercise a system of interactive experiments to verify concepts of advanced ATC systems using fast-time and real-time computer simulations.

The types of experiments to be investigated with the TSC simulation include, for example: strategic control concepts where aircraft are assigned four-dimensional (4-D) route-time profiles developed on the ground prior to flight (Refs. 2 - 4); sequencing, spacing and flow control concepts for regulating the traffic volume in the congested terminal area (Refs. 5 - 8); and separation assurance concepts such as intermittent positive control (IPC) and collision avoidance systems (Refs. 5, 9, 10).

The ATC-oriented program is planned to extend over a period of several years. Since continuing investigations are expected to provide new ATC knowledge, the programs created for the simulation are being made extremely flexible and easy to expand and change. In addition, as new experiments are defined, the simulation programs must be adapted to provide the user with the necessary tools for his purpose.

The present report presents the results of a study conducted by Aerospace Systems, Inc. (ASI) to provide more realistic error models for the TSC simulation. The original ASI objective was to evaluate selected control strategies for satisfying 4-D guidance requirements and to determine the effects of the more important system errors by simulation. However, it became apparent that the error models themselves could easily dominate the results of such an analysis. Consequently, the ASI effort concentrated on developing more sophisticated models of the dominant functional error sources to support the ATC systems evaluation experiments planned for the TSC simulation.

The next section of the report presents a broad overview and background of the present ATC simulation. The requirements for certain improvements in the simulation are mentioned and the general philosophy followed in designing the revised models is discussed. The next four sections present the revised error models for the simulation: Section 3 describes the motions of the aircraft; Section 4 presents the Air Data System errors; Section 5 describes the Navigation System Models; and Section 6 presents the Ground Surveillance and Radar Tracking models. The nomenclature used in these models is defined in the front of the report. This nomenclature and the corresponding units are consistent with that used in the analysis and operations of ATC systems. In Section 7, various features of the revised models are discussed, and some comparisons are made with the previous models. The significant conclusions of the study and suggested applications for the revised models are presented in Section 8. Finally, a comprehensive list of References and a Bibliography appear, upon which much of the modeling was based.

SECTION 2

BACKGROUND

This section presents some background for the development of the ATC error models described in the subsequent sections of the report. The present TSC ATC simulation is reviewed and the need for certain revisions is indicated. The philosophy adopted for developing the revised models is discussed briefly.

2.1   ATC SYSTEM MODEL

A general block diagram of an air traffic control system as it applies between a single aircraft and controller is shown schematically in Figure 1. The target aircraft submits a flight plan request, $\underline{F}^t$, to the sector controller who in turn issues a set of commands in the form of a clearance, $\underline{F}^c$, to the aircraft for execution. The clearance would normally consist of a route for the aircraft to follow and an altitude and airspeed to maintain to prevent conflict with any other controlled aircraft. Under vectoring control in the terminal areas the clearance would specify a heading to maintain instead of the route. For advanced control concepts, the clearance might specify a groundspeed or the times at which to cross certain fixes. For collision avoidance, the clearance might call for climb, dive or turn maneuvers, followed by a command to resume normal navigation.

The air data system provides the aircraft commander with information about the heading, altitude, altitude rate, airspeed and Mach number of his aircraft. The navigation system provides information about the location of the aircraft relative to the desired ground track. Both the air data and navigation systems information contain some errors. The aircraft commander uses the information provided by these systems to control the velocity vector $\underline{V}_a$, of the aircraft relative

- 3 -
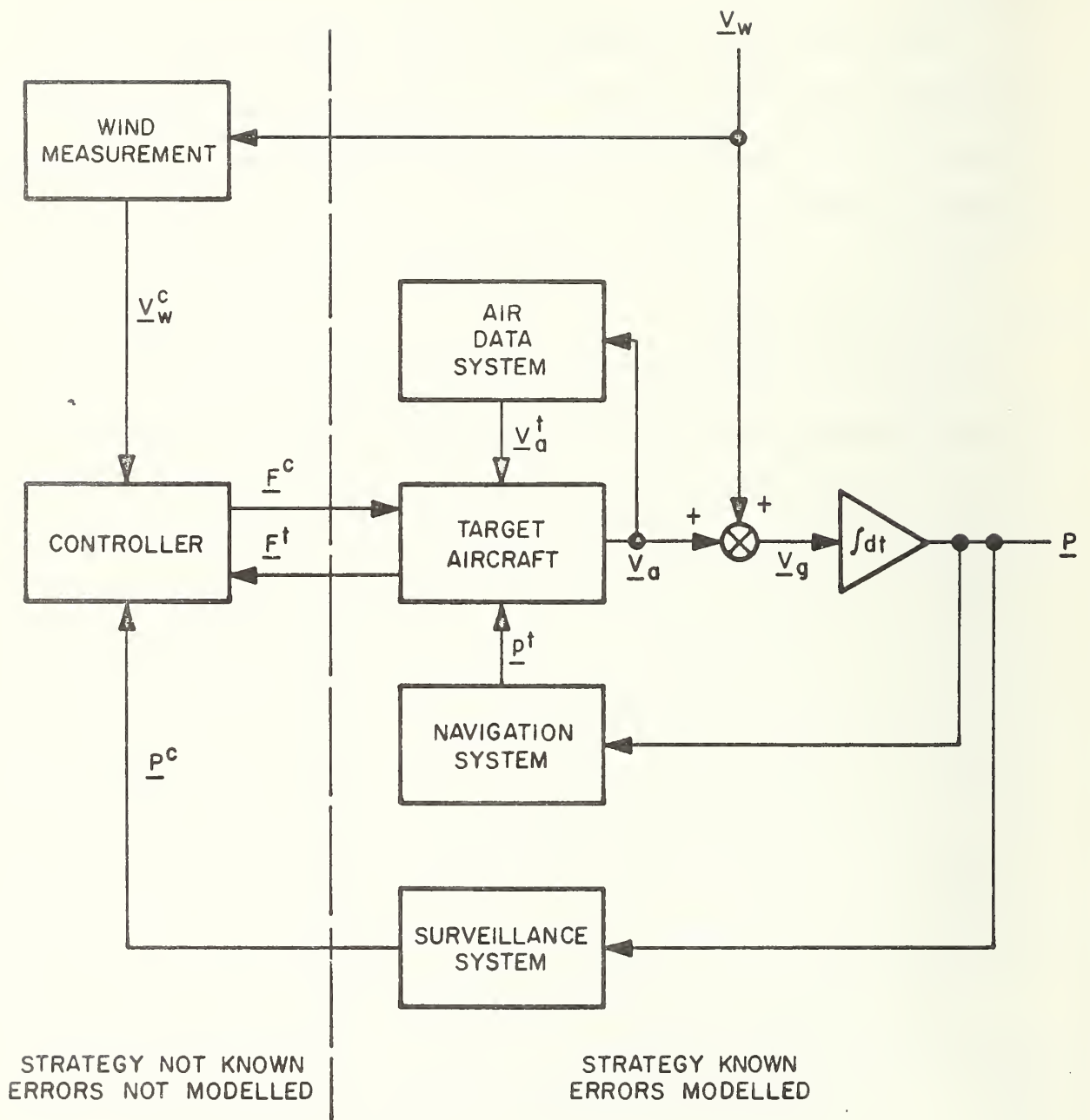
Figure 1. General Air Traffic Control System for a Single Aircraft.

to the air mass, in a manner which he believes will result in adherence to his clearance. In so doing, he uses control strategies which, fortunately, are fairly standard and repeatable.

The groundspeed of the aircraft $\underline{V}_g$, is the vector sum of the airspeed and the wind, $\underline{V}_w$. $\underline{V}_g$ integrates into aircraft position relative to the ground, $\underline{P}$. The positions of target aircraft are sensed by the surveillance system and the information is made available to the sector controller. The sector controller also has some knowledge of the wind, $\underline{V}_w{}^c$, through the weather observations and forecasts. The surveillance information is used to effect changes in the clearances given to the target aircraft.

The net result of various advanced control strategies which might be used by the sector controller is now not known, nor is the effect of system errors on the operation under any given strategy. The overall goal of the TSC effort is to be able to establish these relationships by simulation of the system.

2.2   ATC SIMULATION

The ATC simulation laboratory consists of a PDP-10 digital computer facility and a display system, which uses a DDP-516 computer coupled to an ADDS/900 display unit (Ref. 1). The simulation uses the PDP-10 as the ground-based data acquisition and command and control system, with the DDP-516 computer as the display processor, (Fig. 2). Basically, the functions that are performed by the PDP-10 computer are: (1) simulation of aircraft traffic including models for the pilot, aircraft, terminal area, and environment; (2) control of traffic with automation and decision-making algorithms; (3) manipulation of data files and control to update the display list; (4) scenario generation for each simulation; (5) data recording and reduction; (6) controller/pilot-aircraft command processing; and
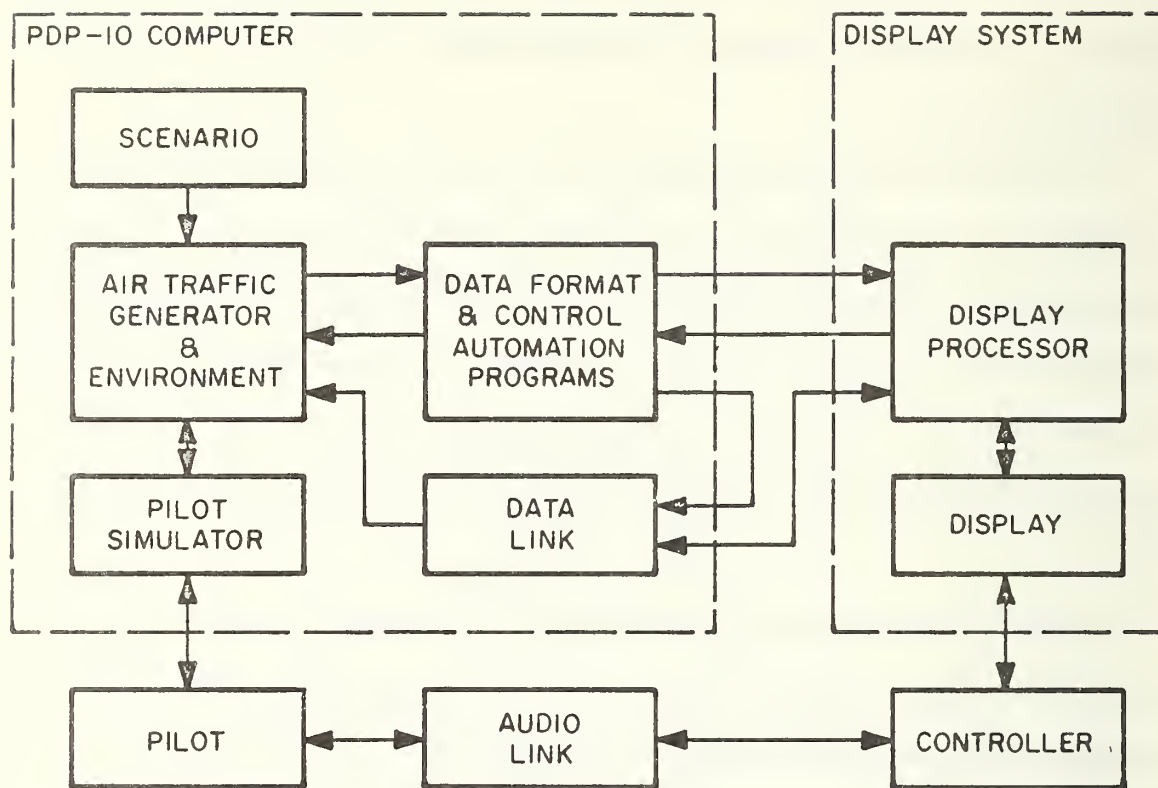
Figure 2. Air Traffic Control Simulation.

(7) flight strip printing. The functions performed by the display processor are:
(1) generation of synthetic background video maps; (2) display file maintenance;
(3) display refreshing: (4) I/O handling for data entry devices; and (5) controller
command execution.

The simulation software has four basic elements (Ref. 1): traffic generation,
sky and terminal environment, pilot module, and control module. The traffic
generator module contains the driving mechanism of the model and introduces flight
characteristics, update timing and sequencing characteristics. A scenario generates
aircraft arrivals and departures and introduces all of the circumstances required
to simulate special events such as airborne equipment failures, runway closures

and reversals, and missed approaches. The environment module includes flight characteristic limits, control response, aircraft errors, and a geographical section that contains position and route definitions. The pilot module accepts pilot commands for heading, speed, and altitude and then implements these commands to the aircraft. The intent of the pilot module is not to model a pilot but to allow an individual to interface the audio commands of the controller to the digital input required by the PDP-10. The controller is provided with a realistic display of traffic and can issue commands to a pilot through an audio link or a simulated data link. Details of the simulation program, Route Oriented Simulation System (ROSS), are contained in References 11 and 12. A brief review of the error models in ROSS is presented next.

The wind environment was represented by layers of constant winds. The wind speed and direction were constant within each layer, and changed instantaneously between two layers. No vertical winds were included. At ASI's suggestion, ROSS was modified to permit wind speed and direction to be continuous linear functions of altitude.

The aircraft altitude, speed and heading are updated, if necessary, as linear functions of time. The rate of climb, rate of descent, acceleration, deceleration and rate of turn are all constant parameters for a particular aircraft. Each parameter is chosen from a normal distribution with a specified mean and standard deviation appropriate for the aircraft type. No dynamic response is included in the motion module; i.e. there is no lag in responding to a command, and no overshoots of the commanded value are allowed. For example, if the altitude change overshoots the desired altitude, the exact altitude is set equal to the desired altitude. However, pure time delays can be introduced to represent communications delays, for example. Fixed instrument bias errors can be represented by selecting the com-

manded altitude, heading or airspeed from specified random distributions.

The new airspeed and wind components are added to obtain groundspeed components. The aircraft position is then updated by extrapolation from its previous value, using the new groundspeed components. If the aircraft is being observed by radar, the range and bearing errors (each defined by a mean and standard deviation) are determined, and the noisy position coordinates relative to the radar site are calculated. When a navigation station is being used, a first-order noise process (with a 0.03 sec time constant) produces sequentially-correlated range and bearing errors, which are converted to noisy position estimates.

A homing mode of navigation is provided in which the aircraft flies directly to a specified position. If the aircraft is more than two miles from the homing position, the heading to that position is computed. To account for crosswinds, the drift angle which would result if the aircraft flew on the heading to the homing position is calculated. This drift angle is then applied as a correction to obtain a desired heading compensated for the wind effects. When the aircraft is less than two miles from the homer, a fixed heading is commanded.

2.3   IMPROVED ERROR MODELS

The ROSS program was developed by using relatively simple kinematics to model the target aircraft and by neglecting certain of the errors in the navigation, air data and surveillance systems. In general there is a trade-off to be made between the complexity of the model representing the system and the cost in computer programming and execution time. As one needs to know better the high frequency response of the system, it is necessary to model the system dynamics in greater detail. At the present time the ROSS program generally provides unrealistic dynamic response characteristics at the higher frequencies, i.e. those frequencies having

periods below 30 seconds. The present simulation permits instantaneous changes in attitude and heading rate, for example. This would require a much faster aircraft-pilot response than is physically possible. Consequently, the dynamic response characteristics need to be modified in the high frequency spectrum or, equivalently, for response times below about 30 seconds.

There are several reasons for wanting to extend the capability of ROSS to represent high frequency effects more accurately. One of these is to evaluate various collision avoidance systems, including intermittent positive control. Typical warning times for such systems are less than 30 seconds and separation distances will be under a few thousand feet. Another application of interest is the 4-D guidance system, using clearances which require the aircraft to hit navigation fixes at specified times. The dynamic effect of the wind and the dynamic errors in the navigation system are expected to have a strong influence on how this control strategy can be used. Another interesting application is to investigate strategies for sequencing and spacing. It has been estimated that timing errors of better than 4 seconds are necessary to achieve maximum runway utilization (Ref. 10). The simulation would have to include all effects of that order of magnitude in order to assess the various control strategies.

The purpose of this work has been to expand the models to the right of the dashed line in Figure 1 to include important effects having response times longer than one or two seconds. The philosophy has been to introduce accuracy and realism to the greatest extent practicable while minimizing the requirement for extensive computation. In most cases the target dynamics depend strongly on the control strategy used by the aircraft commander in following his clearance. Fortunately, pilot procedures for instrument flight are well standardized by FAA guidelines and regulations. Every effort has been made to have the analytic models reflect as nearly as practicable the actions taken by aircraft commanders in the

real world. The models have been developed by pilots familiar with instrument operations, using their judgement where necessary to estimate the magnitude of system parameters. It has been assumed that all clearances are executed upon receipt; communications delays in receiving clearances have not been modeled, but could be included by using the pure delays presently available in ROSS.

The dynamics of the aircraft have been modeled on the basis of physical laws to the extent practicable. Dynamical modes of the aircraft which would be suppressed by automatic or human pilot damping have been neglected. Errors in the air data system are modeled as instrument biases. The navigation system errors are modeled separately for the kind of navigation system under consideration. Errors and loss of information due to both geometry and propagation are included. Where necessary, errors are time-correlated in order to provide realistic system response. The surveillance system includes the same type of sensing errors in addition to the general algorithms used in the third-generation ATC system tracking software.

A note of caution is appropriate regarding the units used in the error models. The primary input and output quantities (e.g. range, altitude, airspeed, rate of climb) have been expressed in the standard terms used in the ATC environment (e.g. nautical miles, feet, knots, feet per minute). Intermediate variables, however, use feet and seconds as the basic length and time units. Consequently, the reader must be careful to avoid confusing these terms. In several places the models contain specific numerical values to convert quantities having dissimilar units.

SECTION 3

TARGET DYNAMICS MODEL

The target dynamics model provides the means of representing the motion of each aircraft (target) in the simulated ATC system. The development of appropriate target dynamics models involves a tradeoff between realism and computational requirements. If unlimited simulation resources were available, the ideal situation could be a complete six-degree-of-freedom simulation of each aircraft in the system, including realistic aerodynamics, engine characteristics and a full cockpit. Obviously, this is not a feasible alternative, and would not be required for the experiments being proposed for the TSC simulation.

On the other hand, the motion update model presently existing in the simulation does not include any dynamic response of the targets; e.g. a commanded change in altitude is immediately followed by a constant rate of climb until the new altitude is precisely attained (perhaps with some steady-state bias error from the altimeter). The target dynamics model presented in this section will provide the simulation user with a compromise between realism and computational simplicity. The target dynamics model has also been developed to be as general as possible, so as to require minimum changes to represent the entire spectrum of aircraft using the ATC system. The representation of a single engine general aviation aircraft or a military fighter is determined by the selection of an appropriate set of performance parameters and response time constants.

Figure 3 shows a general block diagram of the target dynamics model. The inputs include commanded altitude (h_c), commanded airspeed (V_c) or Mach number (M_c), and commanded heading (ψ_c) or track. Disturbances entering the model include winds, air data system errors and navigation system errors. The outputs

AIRCRAFT PARAMETERS

TARGET DYNAMICS MODEL

h_c

V_c

M_c

ψ_c

TRACK COMMAND

h

V_a

M

ψ

χ

V_g

∫

X

Y

WINDS, AIR DATA & NAVIGATION SYSTEMS OUTPUTS
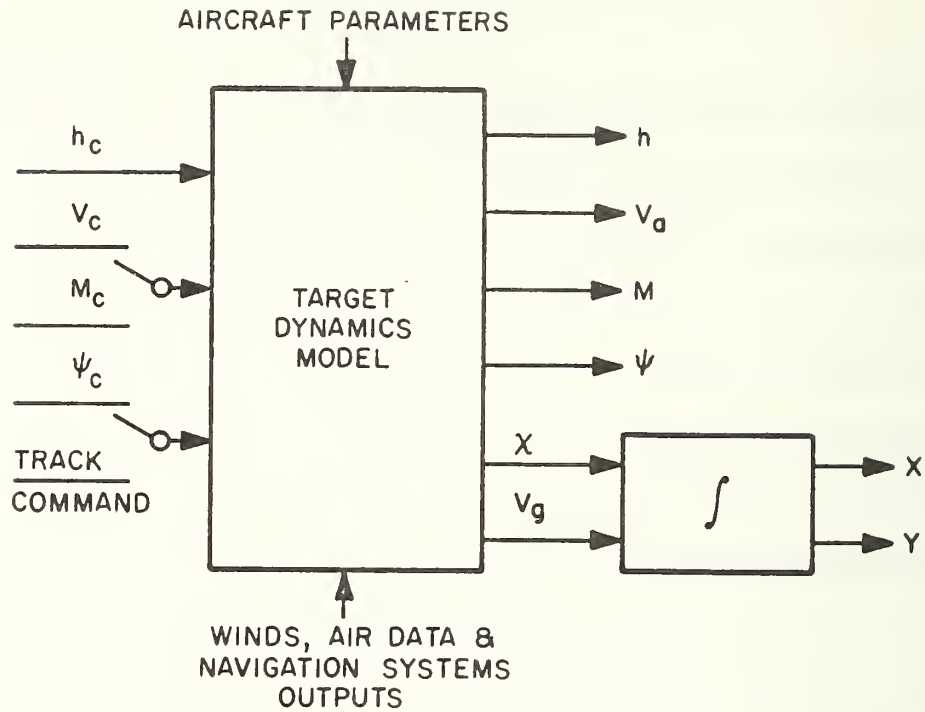
Figure 3. General Block Diagram of Target Dynamics Model.

are the target's true altitude (h), airspeed (V_A), Mach number (M), heading (ψ), ground speed (V_g), ground track angle (χ), and horizontal position coordinates (x,y). Individual elements of the target dynamics model are discussed in detail below according to the commanded input. Nomenclature is defined at the beginning of the report.

3.1 ALTITUDE COMMAND

A block diagram of the altitude command loop is shown in Figure 4. The box labelled "climb/descend logic" generates an altitude rate command based on the current error e_h between the commanded and indicated altitudes. If this
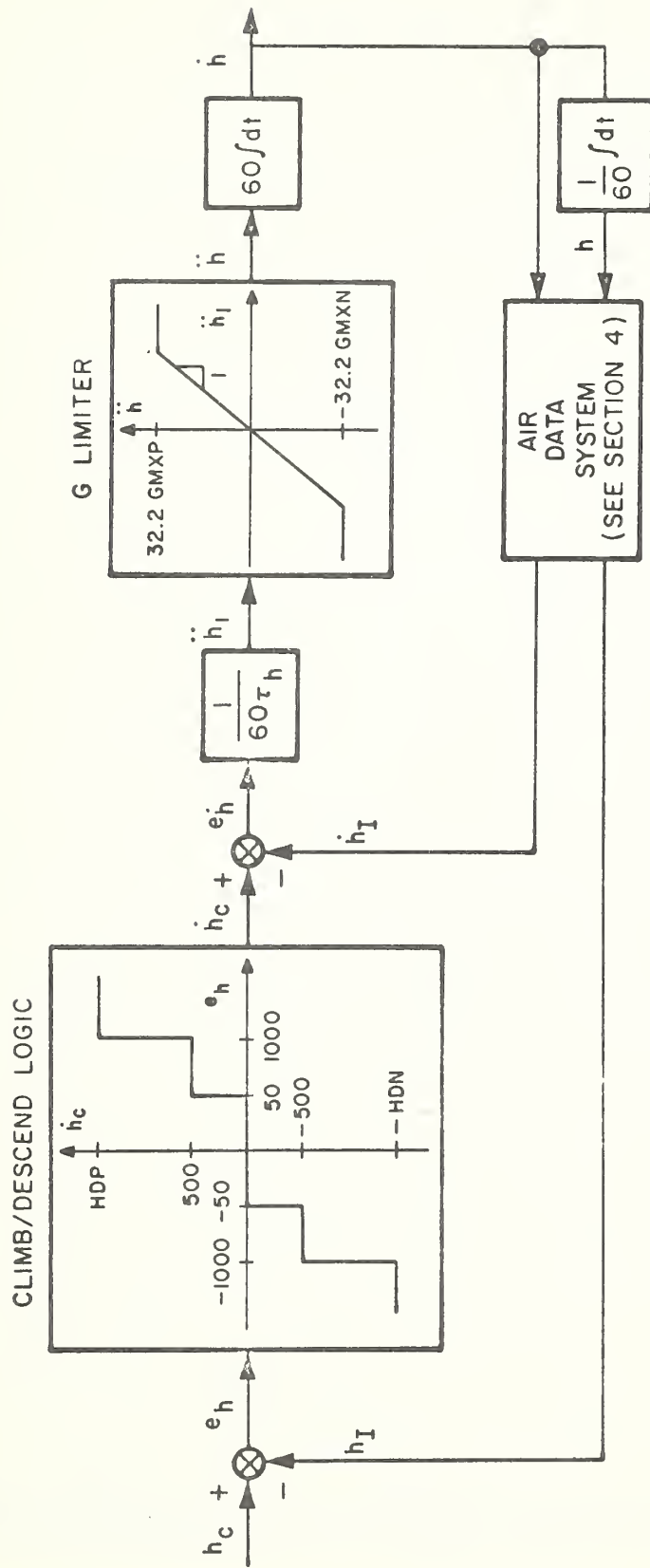
Figure 4. Block Diagram of Altitude Command Loop.

error is greater than 1,000 ft, the best rate of climb or descent (HDP or HDN) is commanded (Ref. 13). The parameters HDP and HDN are functions of the aircraft type and the true altitude. When the aircraft is within 1,000 ft of the commanded altitude, the commanded rate is 500 ft/min. The altitude tolerance is shown as 50 ft; i.e. when the altitude error is less than 50 ft, no corrective action is taken.

The commanded altitude rate $\dot{h}_c$ is compared with the indicated $\dot{h}_I$, and any difference is used to generate a suitable vertical acceleration. The altitude rate feedback loop represents a first-order lag response with a time constant τ_h, and having constraints (GMXP and GMXN) on the magnitude of the vertical g-loading. The output of the box labelled "G limiter" is the true vertical acceleration, which is integrated once to give true altitude rate, and again to give true altitude. Instrument errors are introduced in the air-data system which provides the indicated values h_I and $\dot{h}_I$.

With appropriate values of the parameters HDP, HDN, GMXP, GMXN, and τ_h, the model provides a reasonably accurate dynamic representation of the target response to an altitude command. The values of the parameters given later in this section (Table 1) are for normal enroute or terminal operation. They do not adequately represent situations such as collision avoidance or landing approach, when response times would be shorter and when normal constraints might be ignored.

The altitude command model depicted in Figure 4 is based on normal control by a typical pilot. However, no two pilots and no two aircraft will ever have identical characteristics. For added realism, the various model parameters should be selected from an appropriate random distribution provided by the user. In this way, the behavior of each target in the simulation will be unique. In certain situations, particularly landing approach, the climb/descent logic might

require special modification. For example, the rate of descent during final approach should be a function of groundspeed in order that the Minimum Descent Altitude (MDA) or Decision Height (DH) be reached at the correct distance from the runway.

The equations of motion of the model can be integrated analytically for closed-form solutions, since $\dot{h}_c$ will be piecewise constant. If the "g limits" are not in effect, the altitude rate and altitude are given by:

$$\dot{h}(t) = \frac{1}{K_{\dot{h}}} \left\{ \dot{h}_c(t_1) - e_{\dot{h}}(t_1) \exp[-(t - t_1)K_{\dot{h}}/\tau_h] \right\} \tag{1}$$

$$h(t) = h(t_1) + \frac{1}{60\, K_{\dot{h}}} \left\{ \dot{h}_c(t_1)[t - t_1] - \tau_h[\dot{h}(t) - \dot{h}(t_1)] \right\} \tag{2}$$

where t_1 is the time of the last update and $K_{\dot{h}}$ is a scale factor error in the air data system (see Section 4.2). When the "g limit" is in effect, the equations are even simpler:

$$\dot{h}(t) = \dot{h}(t_1) + 60\, \ddot{h}(t_1)[t - t_1] \tag{3}$$

$$h(t) = h(t_1) + \dot{h}(t_1)[t - t_1]/60 + \ddot{h}(t_1)[t - t_1]^2/2 \tag{4}$$

The latter equations could be used when the g limit is not in effect, thereby introducing a maximum error of less than 100 ft/min in $\dot{h}(t)$. The step size used in the simulation $(t - t_1)$ is a constant which is generally set at 1 second in the present version. The exponential function in Equation (1) could be approximated by the first three terms in the series expansion to conserve computer time. This simplification would result in an error of about one percent or less. If the first two terms of the series are used, Equation (3) is obtained.

3.2   AIRSPEED COMMAND

In response to an airspeed command, the pilot will adjust the thrust

and/or drag to provide the desired longitudinal acceleration or deceleration. However, the resulting acceleration/deceleration acts upon the ground-referenced (inertial) velocity of the aircraft, which is seldom the same as the air-referenced velocity due to the effects of winds. Similarly, lateral accelerations in turning maneuvers will also affect the airspeed response as a result of crosswinds. This coupled airspeed-heading response will be discussed next.

Figure 5 depicts the situation of an aircraft flying through a wind. The wind magnitude is V_w, blowing from the magnetic direction θ_w. The aircraft heading in the
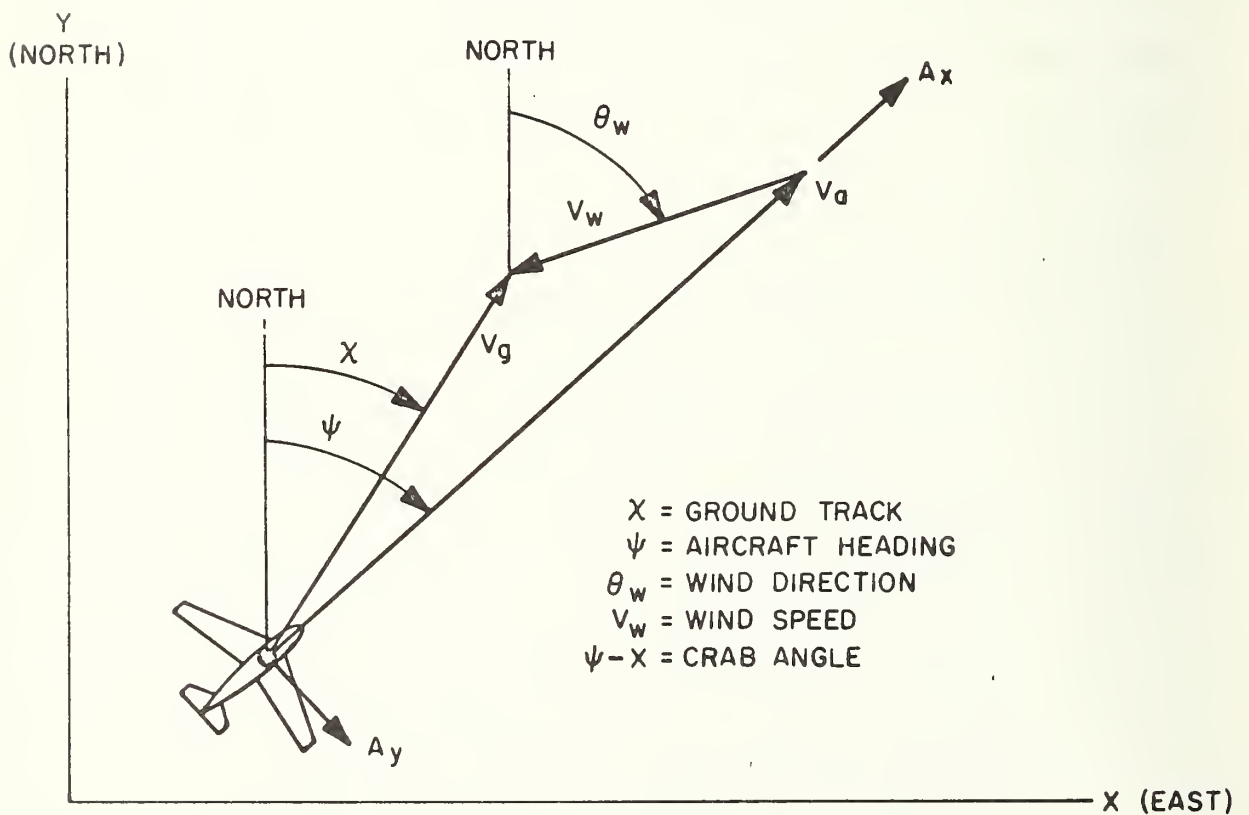
Figure 5. Geometry and Nomenclature for an Aircraft Flying through a Wind.

- 16 -

air mass is ψ, and the airspeed is V_a. The resulting groundspeed is V_g and the ground track angle is χ. The longitudinal acceleration A_x applied to the aircraft is proportional to the difference between the thrust and the drag, both of which act parallel to V_a in coordinated flight. The lateral acceleration A_y results from a co-ordinated bank which rotates the aerodynamic lift vector about V_a. The equations of motion in ground-referenced coordinates are:

$$\dot{V}_g = A_x \cos(\psi - \chi) - A_y \sin(\psi - \chi) \tag{5}$$

$$V_g \dot{\chi} = A_x \sin(\psi - \chi) + A_y \cos(\psi - \chi) \tag{6}$$

By geometry, the airspeed and heading are:

$$V_a = [V_g^2 + V_w^2 + 2 V_g V_w \cos(\theta_w - \chi)]^{1/2} \tag{7}$$

$$\psi = \chi + \sin^{-1}[(V_w/V_a) \sin(\theta_w - \chi)] \tag{8}$$

Note that if there is no wind ($V_w = 0$), $V_a = V_g$ and $\psi = \chi$.

Figure 6 presents the general block diagram for the coupled aircraft response to air speed and heading commands. The heading command loop shown in the lower part of the diagram will be discussed later in this section.

In the airspeed command loop, an error between the commanded and indicated airspeed e_V in excess of 2.5 knots results in a longitudinal acceleration command (e.g. throttle movement). This acceleration command is assumed to be proportional to airspeed errors of 20 knots or less; for error magnitudes of more than 20 knots, maximum acceleration (ACR) or deceleration (DCR) for the aircraft type is commanded.

Due to pilot-aircraft-engine response time, the commanded acceleration/deceleration is not immediately achieved. The inner loop from A_{x_c} to A_x represents

- 17 -

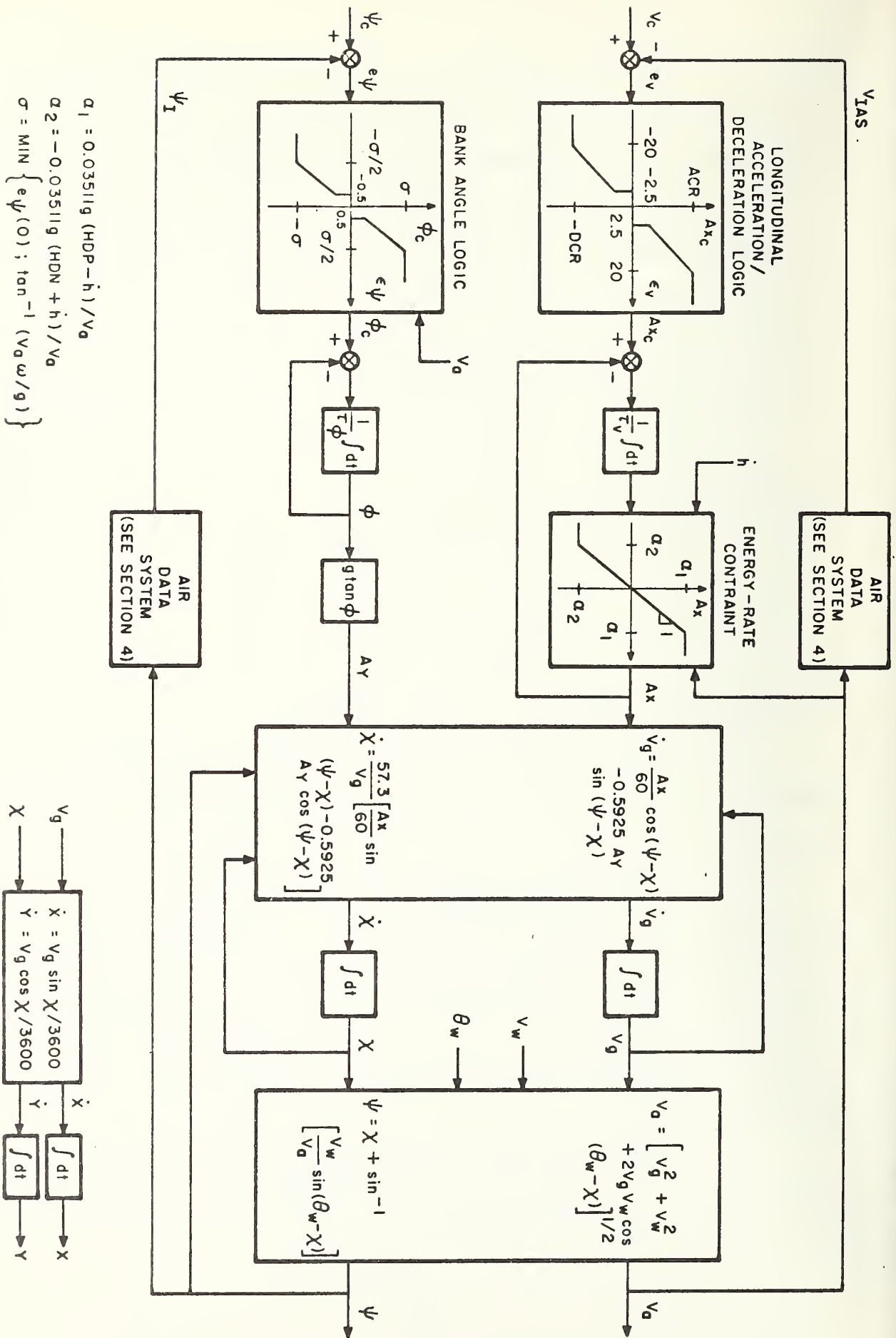Figure 6. Block Diagram of Coupled Airspeed Command and Heading Command Loops.

a first-order lag response with a time constant of τ_V. The block labeled "Energy Constraint" limits the actual longitudinal acceleration (or deceleration) if the aircraft is simultaneously climbing (or descending). The acceleration limit is determined by the excess of the maximum rate of climb (or descent) capability over the actual rate. When the aircraft is climbing at its maximum capability, it has no additional power available for acceleration. Similarly, during a maximum rate of descent, the pilot cannot simultaneously reduce airspeed.

The next block in Figure 6 resolves the longitudinal and lateral accelerations into components along and normal to the ground referenced velocity. These are integrated to obtain V_g and χ, which are used with the existing wind magnitude and direction to give the true airspeed and heading angle. In general, the pilot does not control true airspeed, but indicated airspeed, which is based on the difference between dynamic and static pressure measured by the air data system.

The groundspeed is resolved into North and East components, which are integrated to obtain the aircraft coordinates x, y in the ground reference frame. The derivatives $\dot{x}$ and $\dot{y}$, as well as all other derivatives in the target dynamics models are expressed in appropriate units per second.

The velocity and heading response models could be slightly simplified by neglecting the effect of the aircraft "crab angle" $\psi - \chi$ when flying through a crosswind. This would decouple the groundspeed and ground track angle equations. However, since the crab angle can often be 20° or more, this simplification could result in sizable errors, particularly when turning in a wind environment.

The integration of the equations in the velocity and heading response loops of Figure 6 is considerably more complex than in the case of the altitude response. Closed-form solutions, while possible, would be extremely cumbersome.

A simple numerical integration technique, such as Runge-kutta, should provide

sufficient accuracy. An alternative procedure would be to assume that the signal

is constant over the time step interval at a selected point in each loop (e.g.,

A_{x_c} and ϕ_c). Then simpler analytical expressions could be obtained for the remainder

of the loop.

3.3   MACH NUMBER COMMAND

In most jet aircraft, the pilot will often be controlling Mach number instead

of airspeed, particularly during the climbout and cruise phases. The control

technique is essentially the same as for airspeed control, with the exception

that the longitudinal acceleration is adjusted according to the error in Mach

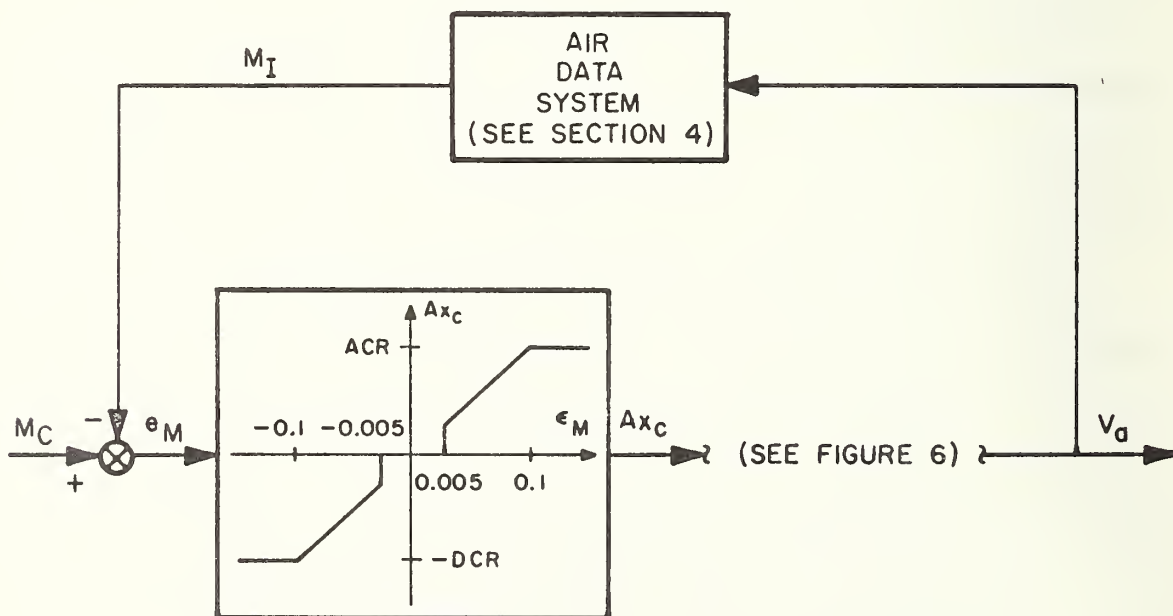number. Figure 7 shows the control logic for the Mach number command loop.

Figure 7. Block Diagram of Mach Number Command Loop.

During this mode of operation, the A_{x_c} from Figure 7 is used in place of that generated in Figure 6. Otherwise, the control loop of Figure 6 is unchanged for Mach number commands.

The Mach number tolerance shown is 0.005, which corresponds to a true airspeed tolerance of the order of 3 knots. Linear control is assumed for Mach number errors between 0.005 and 0.10, and full control for errors in excess of 0.10 Mach number.

3.4   HEADING COMMAND

The heading command loop shown previously in Figure 6 applies whenever the pilot is attempting to maintain a desired magnetic heading, as when he is being vectored by ATC for example.

Any difference between desired and indicated heading is used to generate a bank angle command ϕ_c, according to the block labeled "bank angle logic". A very close tolerance on heading is usually maintained; the value selected in Figure 6 is shown as 0.5°. Any heading errors greater than this are corrected. The maximum commanded bank angle σ depends upon the size of the initial heading error, $e_{\psi}(0)$, and the standard-rate turn bank angle, $\tan^{-1}(V_a \omega/g)$. If the desired heading change is less than the standard-rate turn bank angle, the maximum bank angle command is equal to the initial heading error; otherwise, the bank angle for a standard-rate turn is used. The initial bank angle command is maintained until the heading error is reduced to one-half the bank angle command $\sigma/2$ (Ref. 13). Then linear bank control is used until the heading error is within tolerance. The value of σ should be recomputed whenever a new heading command is issued.

The actual bank angle is approximated by a first-order lag response to the commanded value. The lag time constant approximates the pilot and aircraft

- 21 -

response to the bank command. The resulting bank angle produces a lateral acceleration by rotating the lift vector out of the vertical plane. If the aircraft angle-of-attack is adjusted to keep the vertical component of lift equal to the aircraft weight, the lateral acceleration is $A_y = g \tan \phi$.

As explained previously, the longitudinal and lateral accelerations are resolved into ground referenced coordinates and integrated to obtain V_g and X, which then determine V_a and ψ. NOTE: ground track and heading angles must be restricted to the range

$$0^{\circ} < X, \psi \le 360^{\circ}$$

However, in the integration of the $\dot{X}$ equation, it may be necessary to use an intermediate variable which is unrestricted, and then add or subtract 360° as required to obtain X.

3.5   COURSE TRACKING COMMAND

During the greatest part of most flights, it is necessary for the pilot to follow a given course over the ground by reference to various navigation systems. The most frequently-used navaid for at least the near future is the VOR/DME system which defines the low altitude Victor Airways and high altitude Jet Routes.

Figure 8 defines the nomenclature used for the course tracking model. The figure shows the situation of an aircraft attempting to track outbound on the θ_c radial of a VOR/DME station. The object of the course tracking loop is to null the cross track distance $d = R \sin (\theta_c - \theta)$. However, to prevent large overshoots of the desired track, some rate damping must be provided, either in the form of $\dot{d}$ or ground track error, $X - \theta_c$. Since in most cases neither of these is readily available aboard the aircraft, the difference between heading and desired track,
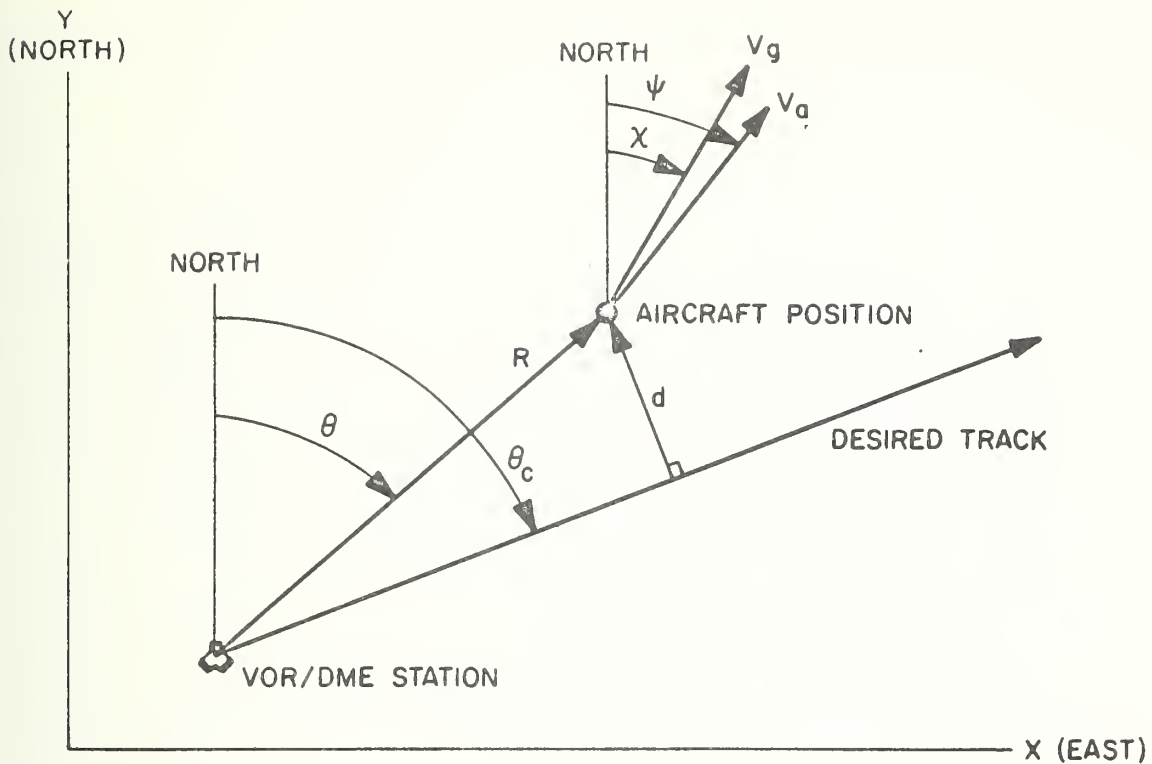
Figure 8. Geometry and Nomenclature for Course Tracking Model.

$\psi - \theta_c$ (i.e., the zero-wind ground track error), is frequently used as a substitute.

A model for this process is analyzed in Kayton and Fried (Ref. 14) and is shown in block diagram form in Figure 9. The analysis of this model neglects the bank angle delay, which is of the order of 1 - 2 seconds, and assumes the aircraft is in the vicinity of the desired course. The equations of motion for the no-wind response of the tracking loop are linearized, to produce a second-order system with natural frequency ω_n and damping ratio ξ_n. The values of ω_n and ξ_n can be adjusted by the choice of the gains K_1 and K_2 as indicated in the figure. A reasonable response is obtained with $\omega_n = 2$ rad/min and $\xi_n = 0.7$, which is equivalent to setting the gains

- 23 -
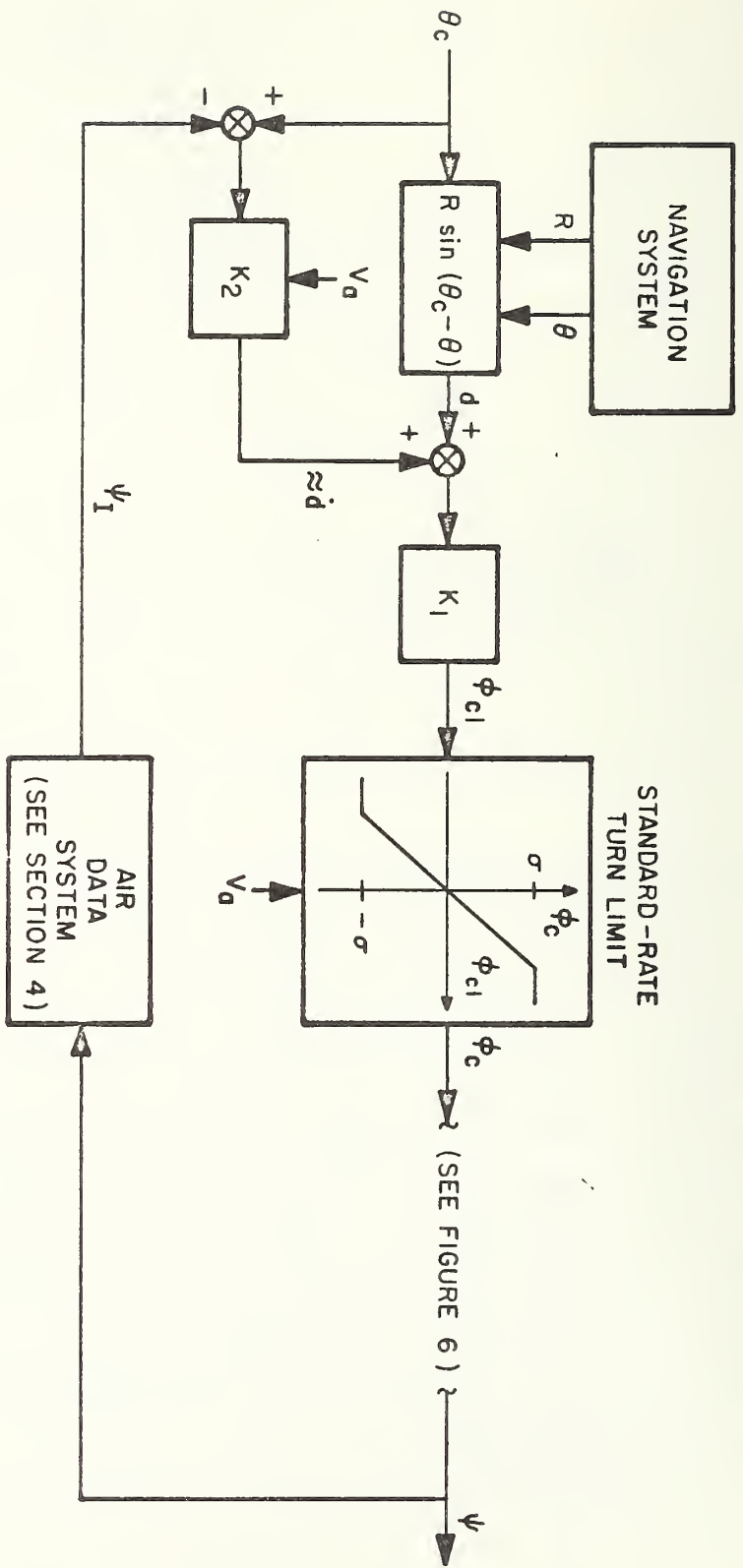
Figure 9. Block Diagram of Course Tracking Model.

$$\omega_N \doteq \sqrt{gK_1}$$

$$\xi_N \doteq gK_1 K_2 / 2V_a$$

$$\sigma = \tan^{-1}(V_a \, \omega/g)$$

$$K_1 = 12.0 \ \text{deg/nm}$$

$$K_2 = 0.000204 \ V_a \ \text{nm/deg}$$

The effect of the wind will be to cause slight variations typical of the variation between pilots or autopilots. The value of K_2 is made a function of V_a to avoid specifying different gains for various speed aircraft. The commanded bank angle for the course tracking model must be limited to prevent exceeding a standard rate turn, where σ is the magnitude of the bank angle that produces a standard rate turn. The resulting bank angle command ϕ_c is then used in the heading loop of Figure 6 in place of the value shown there for heading commands. The dynamics of the bank angle response introduce additional variations between aircraft which are typical of the real world. As a result the actual response will differ slightly from that of a linear, second-order system with natural frequency ω_n and damping ratio ξ_n.

The model for tracking with a navigation system that displays off-track displacement as a linear distance instead of an angle is only slightly different from the course tracking model discussed above. This could be used, for example, with an inertial navigator or an RNAV system. The cross-track error, d, would come directly from the navigation system. The damping signal could also be obtained directly from the navigation system but that is not necessary.

The tracking model in Figure 9 will settle down to zero cross track error if there are no winds. However, in the presence of a cross wind, the steady-state crab angle will result in a small cross track bias error $d_{ss} = -K_2(X_{ss} - \psi_{ss})$. This bias could be eliminated by means of a washout filter or by adding a term proportional to the integral of d to the bank angle command. However, the additional complexity does not seem to be warranted for the next stage in improving the ATC simulation.

3.6   COURSE INTERCEPT COMMAND

In most instances, the aircraft will be either vectored to the desired course, or transferring from one leg of a route to another with relatively small changes in track angle. In these situations, the tracking model will be perfectly satisfactory. However, the pilot will occassionally be directed to intercept and maintain a given course which may be outside the valid region of the linear tracking model. In the latter situations, some logic is required to guarantee proper intercept of the commanded course.

In most course intercept situations, it is expedient to achieve track with the least delay. For the idealized case of constant airspeed, constant altitude, no winds and instantaneous bank angle response, the minimum-time intercept paths consist of segments of circles and straight lines (Ref. 15). A closed-loop feedback control chart can be obtained for this case showing the optimum bank angle $(+\sigma, 0, -\sigma)$ as a function of cross track error, d, and ground track error, $\theta_c - \psi$ (see Fig. 8). In the more realistic situation being considered here, a simpler sub-optimum control chart can also be defined which will always place the aircraft near the desired course where the course tracking model can be correctly applied.

The sub-optimum minimum-time course intercept logic is shown in Figure 10. The ordinate has been normalized with respect to the radius of a standard-rate turn, V_a/ω. In the regions labeled "track mode" the course tracking model discussed above will be used to determine the bank angle command. Note these regions extend to two turn radii either side of the desired course, and to a heading angle within 90° of the course. Outside of these regions, full right bank ($\phi_c = +\sigma$), full left bank ($\phi_c = -\sigma$) or straight flight ($\phi_c = 0$) is commanded until the track mode regions are penetrated. For large initial cross track errors, this logic will call for a standard rate turn of minimum heading change until the aircraft is headed
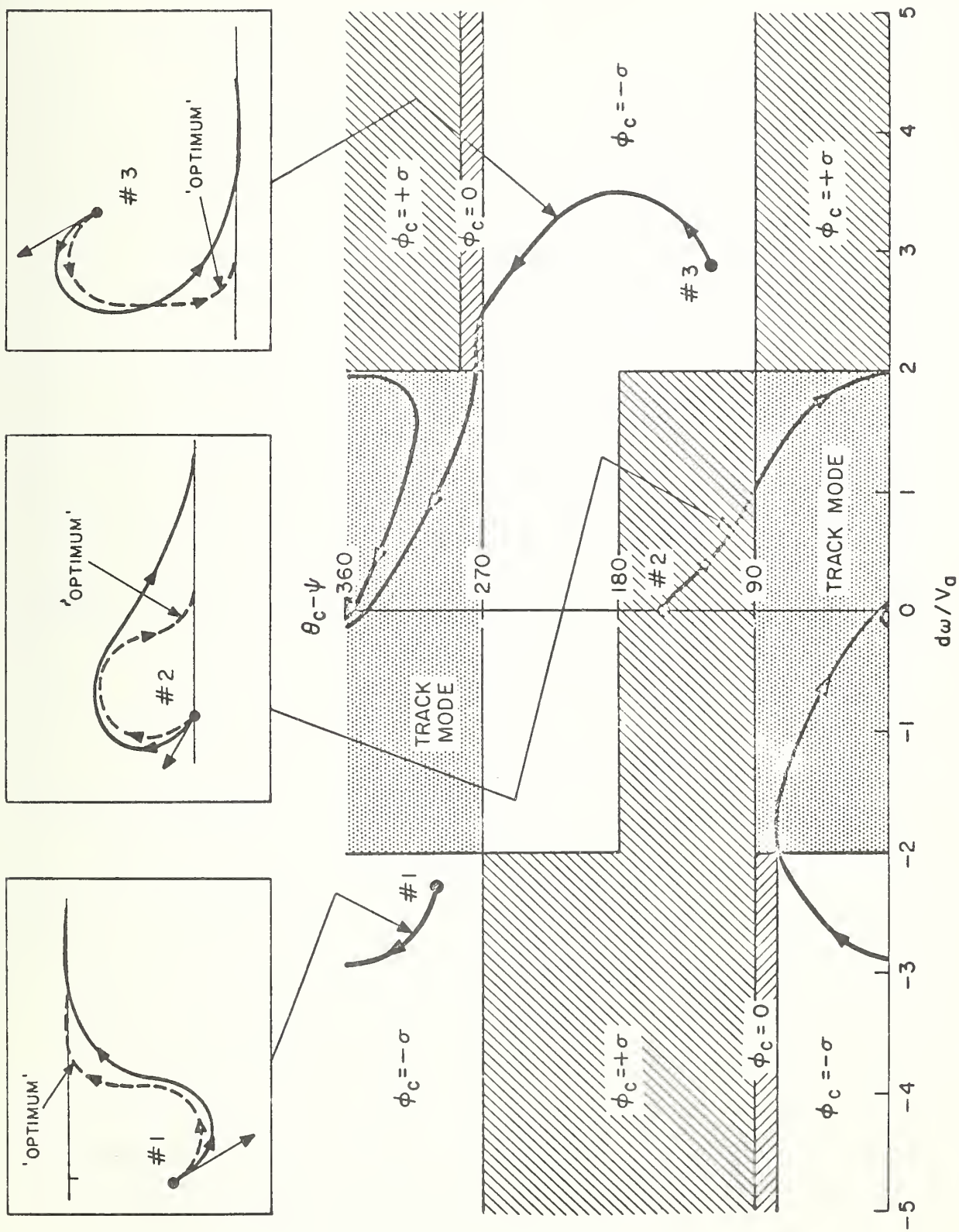
Figure 10. Bank Angle Logic for Course Intercept.

nearly perpendicular to the course; the aircraft will then fly straight until it is within 2 turn radii, after which it will switch into the tracking mode of operation.

The width of the $\phi_c = 0$ regions in Figure 10 is adjustable, but 10° seems to be satisfactory. These regions are expansions of the straight lines at $\phi_c - \psi = 90^o$ and 270° in the idealized optimum situation. The size of the track mode region was somewhat arbitrarily chosen for ease of implementation. In actuality, maximum bank angle will be commanded in a large portion of this region due to the bank angle constraints in Figure 9.

Three example course intercept trajectories are shown in Figure 10 to illustrate the performance of the logic. The ground tracks for these trajectories relative to the desired course are sketched in the upper portion of the figure. For comparison, the corresponding optimum turns are also sketched. The major differences between the two paths are a delay in achieving the standard turn rate for the suboptimum case, and a lower frequency response with a slight overshoot within the tracking mode region.

3.7   NOMINAL TARGET PARAMETERS

A number of aircraft-related parameters are required to utilize the target dynamics model just described. Appropriate values of these various parameters should be specified by the simulation user for his particular investigation. However as a guide to the user, Table 1 contains suggested nominal values of the parameters for a variety of aircraft types. As explained earlier in this section, the parameters in Table 1 illustrate typical estimated values for normal enroute operations. These values should not be utilized in general for relatively quick reaction time situations such as collision avoidance. To the extent possible, the aircraft types and parameters presented are consistent with those used in previous DOT simulations at TSC and

Table 1. Typical Aircraft Parameters for Target Dynamics Model

Type Aircraft	Units	Propeller				Turbo-Prop			Jet					
									Exec.	Commercial			Military	
		Lt. Sgl.	Lt. Twin	Med. Twin	Hvy. Twin & Four	Lt.	Med.	Hvy.		Med.	Std.	Hvy.		
Category		1	2	3	4	5	6	7	8	9	10	11	12
HDP (0-10,000')	ft/min	1,000	1,500	1,500	1,000	2,000	2,000	2,000	1,500	1,500	1,500	1,500	10,000
(10,000'-20,000')	ft/min	500	800	1,200	2,000	2,500	2,500	3,000	2,500	3,000	3,000	1,500	10,000
(20,000'-30,000')	ft/min	0	0	0	0	0	2,500	3,000	2,500	3,000	3,000	3,000	10,000
(30,000'-40,000')	ft/min	0	0	0	0	0	0	0	2,500	3,000	3,000	3,000	8,000
(above 40,000')	ft/min	0	0	0	0	0	0	0	0	0	0	0	8,000
HDN – Enroute	ft/min	1,000	1,500	2,000	2,000	2,500	2,500	2,500	3,000	3,000	3,000	3,000	5,000
HDN – Terminal	ft/min	1,000	1,000	1,000	1,000	1,200	1,500	1,500	1,500	1,600	1,500	1,600	2,000
HDN – Max.	ft/min	1,500	2,000	2,500	3,000	3,500	4,000	4,000	4,000	4,000	4,000	4,000	15,000
GMXP	g's	0.2	0.2	0.2	0.2	0.2	0.2	0.2	0.2	0.2	0.2	0.2	0.2
GMXN	g's	0.2	0.2	0.2	0.2	0.2	0.2	0.2	0.2	0.2	0.2	0.2	0.2
ACR	kt/min	60	70	70	80	70	80	60	60	60	65	65	90
DCR	kt/min	60	60	60	60	60	60	60	60	60	60	60	90
τ_h	sec	2	2	2	3	3	3	3	3	3	3	3	2
τ_v	sec	2	2	2	3	3	3	3	3	3	3	3	2
τ_ϕ	sec	2	2	2	2	2	2	2	2	2	2	2	2
ω	deg/sec	3	3	3	3	3	3	3	3	3	3	3	3

NAFEC. These values could be permanently included in the simulation to provide default values for those quantities not specified by the user.

As mentioned earlier no two aircraft, even of the same type, are truly identical because of condition, equipment, loading and other factors. Consequently, the parameters presented in Table 1 should be considered as average values. The specific values for a particular simulation target should be selected from a normal random distribution, having a mean as shown in Table 1, with a suggested standard deviation of 10% to 20% of the mean value. However, care must be taken that the selected parameters are always positive.

SECTION 4

AIR DATA SYSTEM MODEL

The aircraft air data system consists of aerodynamic and thermodynamic sensors, some form of computer and various displays. The outputs of the air data system are indicated values of various flight parameters such as altitude, air-speed or Mach number. Although it is not generally considered a part of the air data system, the heading indicator will be included in the air data system model for convenience.

A general block diagram of the air data system is shown in Figure 11. A detailed explanation of the air data system operation is not necessary for the purposes of this model; such a description may be found in other sources (e.g. Ref. 14).
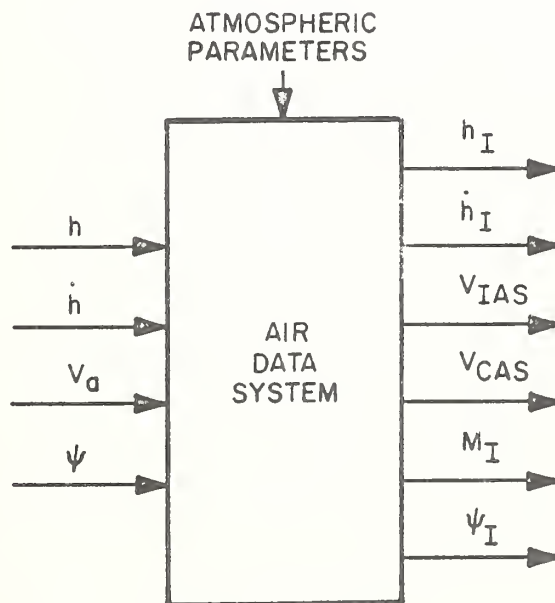

Figure 11. General Block Diagram of Air Data System Model.

The air data system errors generally consist of scale factor errors and biases. Each element of the air data system model includes a reasonably simple representation of the overall error in the indicated quantity.

4.1   ALTIMETER

The barometric altimeter indicates the pressure altitude of the aircraft based on the static pressure measurement and a standard temperature-altitude profile of the atmosphere. Local barometric fluctuations can be corrected for by adjusting the sea-level barometric pressure in flight. The principal altimeter errors are due to static defect, nonstandard temperature-lapse rate and instrument errors.

The static defect is the difference between the free-stream static pressure and the measured value, and is usually not significant at speeds below about Mach 0.4. A static defect is usually calibrated as a function of Mach number, and automatically corrected for by the air data system (c.f. Ref. 16). A typical maximum static defect is 350 ft, with a spread of 100 ft among aircraft of the same type (Ref. 14). A non-standard temperature-lapse will result in an error between true altitude and pressure altitude, but all aircraft will be similarly affected. Therefore lapse-rate errors will not appreciably affect the relative vertical spacing of aircraft, although terrain clearance can be in error as much as several tens of feet per thousand feet of true altitude.

Altimeter instrument errors, including transducer, computer and indicator errors, have been widely discussed (Refs. 17 - 20), especially for altitudes above 30,000 ft. The altitude variation of the instrument error is inversely proportional to the atmospheric density. The SAE design objective is an accuracy of 0.2 percent or 25 ft, whichever is greater (Ref. 21). The latest airline specifications (ARINC 575-3) call for a 3σ instrument error ranging from 15 ft at sea level to

80 ft at 50,000 ft (Ref. 22). It is estimated that the standard deviation of all present altimeters is about 25 ft at sea level.

The altimeter model is based principally on the instrument error discussed above. The indicated altitude is

$$h_I = h + \epsilon_h(h) \tag{9}$$

where the error $\epsilon_h(h)$ is given by

$$\epsilon_h(h) = \epsilon_h(0)[\rho(h)/\rho_0]^{-1} \tag{10}$$

The atmospheric density ratio can be closely approximated as an experimental function of altitude:

$$\rho(h)/\rho_0 = e^{-h/h_1} \tag{11}$$

where $h_1 = 31,186$ ft. The sea level instrument error $\epsilon_h(0)$ for a particular altimeter should be selected from a normal distribution with zero mean and a standard deviation of about 25 ft:

$$\epsilon_h(0) = N[0, 25] \tag{12}$$

4.2   VERTICAL SPEED INDICATOR

The standard vertical speed indicator (VSI), or rate of climb indicator, senses differential changes in the static pressure by means of a calibrated leak. As static pressure changes during entry to a climb or descent, the VSI immediately shows a change of vertical direction. However, until the differential pressure stabilizes, reliable rate indications cannot be obtained. A 6- to 9-second lag normally is required to equalize or stabilize the pressures. The instantaneous vertical speed

- 33 -

indicator is a recent development which incorporates acceleration pumps to stabilize the pressure differential without the usual lag time. Typical VSI errors are estimated to be about 5% to 10% of the altitude rate. ARINC Specification 575-3 (Ref. 22) calls for an accuracy of 30 ft/min or 5%, whichever is greater.

The uncertainty in a particular VSI is modeled as a fixed scale factor error:

$$\dot{h}_I = \dot{h} + \epsilon_{\dot{h}} = K_{\dot{h}} \dot{h} \tag{13}$$

where the scale factor $K_{\dot{h}}$ is selected from a normal distribution with a σ of 5%:

$$K_{\dot{h}} = N[1.0, 0.05] \tag{14}$$

Thus, the absolute error in the vertical speed indicator is given by

$$\epsilon_{\dot{h}} = (K_{\dot{h}} - 1)\dot{h} \tag{15}$$

The pressure stabilization lag time is not included in the model, since altitude rate is not controlled very tightly during transient conditions, and the instantaneous VSI is available if required.

4.3   AIRSPEED INDICATOR

True airspeed, V_a, is the actual speed of the aircraft relative to the surrounding air mass. Of more importance to the pilot, however, is indicated airspeed, V_{IAS}, which determines maximum and minimum safe flying speeds, and on which climb, descent and cruising speed schedules are often based. V_{IAS} is measured directly by the difference between the impact pressure, p_t, sensed by the pitot tube, and the static pressure, p_s:

$$V_{IAS} = 0.5925 \sqrt{2(p_t - p_s)/\rho_0} \quad \text{(kts)} \tag{16}$$

where ρ_0 is the standard density at sea level. Indicated airspeed is related to true airspeed as follows. The static defect and instrument errors correct V_{IAS} to calibrated airspeed V_{CAS}. V_{CAS} is multiplied by $\sqrt{\rho_0/\rho}$ to correct for the density at the aircraft altitude, resulting in equivalent airspeed. A correction which accounts for the compressibility of the air at high altitude–speed regimes corrects equivalent airspeed to true airspeed, V_a. Below Mach 0.8 at 30,000 ft, equivalent airspeed and true airspeed are identical within 7 percent (Ref. 14).

The model for obtaining indicated airspeed from true airspeed is shown in Figure 12. The compressibility correction is neglected since it is small relative
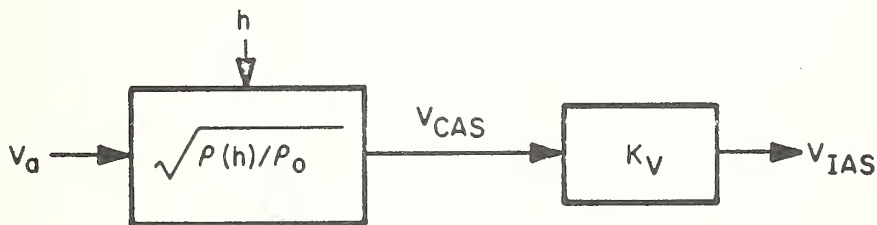
Figure 12. Block Diagram of Indicated Airspeed Model.

to the density correction, and since Mach number rather than V_{IAS} is normally controlled whenever the compressibility is significant. Consequently, true airspeed is converted to V_{CAS} by the density ratio, which can be closely approximated as shown in Equation (11). The instrument error which distinguishes between V_{CAS} and V_{IAS} is approximately proportional to airspeed. Thus, for a particular aircraft, the error in V_{IAS} can be represented by a scale factor K_V selected from a normal distribution:

$$K_V = N[1.0, 0.02] \tag{17}$$

where the standard deviation of 2% is estimated to be typical.

4.4 MACH INDICATOR

Mach number is required in high performance aircraft for defining safe speed ranges, fuel management, jet-engine control, and calculating other aerodynamic quantities. Mach number is the ratio of the aircraft's true airspeed to the local speed of sound. It is generally calculated in flight from the ratio of impact to static air pressure (Ref. 14).

Figure 13 shows the model for indicated Mach number, M_I. The local

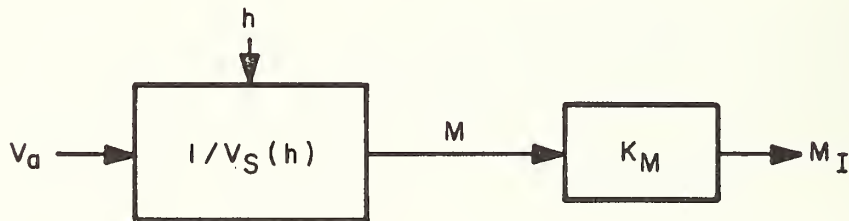Figure 13. Block Diagram of Indicated Mach Number Model.

speed of sound, $V_s(h)$ in knots, can be closely approximated by the expression

$$V_s(h) = \begin{cases} 1.734472 \sqrt{145,501 - h} & , \quad h \leq 36,089 \text{ ft} \\ 573.8 & , \quad h \geq 36,089 \text{ ft} \end{cases} \tag{18}$$

The instrument error in the Mach indicator is approximately 2%, which can be represented as another scale factor.

$$K_M = N[1.0, 0.02] \tag{19}$$

4.5 HEADING INDICATOR

Although the heading indicator is not truly a part of the air data system, it is included here for convenience. The gyroscopic heading indicator provides the pilot's primary direction information. In most high performance aircraft the heading indicator is slaved to a remote compass which continuously maintains the north reference. Less expensive gyros, used in most general aviation aircraft, must be manually reset from the magnetic compass periodically. Thus, the average accuracy of the heading indicators varies considerably among various aircraft. The principal errors are due to inaccuracies in the magnetic compass reference and, for non-slaved instruments, to gyro drift between resettings.

The indicated heading model assumes a constant error ϵ_ψ selected from a normal distribution with zero mean:

$$\psi_I = \psi + \epsilon_\psi \tag{20}$$

$$\epsilon_\psi = N[0, \sigma_\psi] \tag{21}$$

The standard deviation of the heading error, σ_ψ, is estimated to range between about $1°$ (for commercial jets) to $3°$ or more (for smaller general aviation aircraft).

SECTION 5

NAVIGATION SYSTEMS MODEL

A great number of navigation systems have been developed to provide the pilot with position information and/or course guidance (cf. Ref. 14). These range from ground-based radio direction finding to sophisticated self-contained inertial navigation systems. By far the most widely used system at present, and for at least the near future, is the VOR/DME system, upon which the US low-altitude Victor Airways and high-altitude Jet Routes are based. An increasing number of airborne area navigation (RNAV) systems are coming into operation to provide much greater flexibility from the existing VOR/DME system.

5.1   VOR/DME SYSTEM

This system is comprixed of two separate but complementary radio navaids which are normally used in conjunction with one another:

- Very-high-frequency Omnidirectional Range (VOR)
- Distance Measuring Equipment (DME)

The development and operation of these systems has been widely documented in the literature (e.g. Refs. 23 - 30) and will not be repeated here. The VOR indicates the magnetic bearing of the aircraft from the selected ground station, while the DME measures the slant range between them (see Fig. 14).

VOR Model

The correct magnetic bearing from the VOR station to the aircraft is:

$$\theta = \theta_M + \tan^{-1} [(x_a - x_s)/(y_a - y_s)] \tag{22}$$
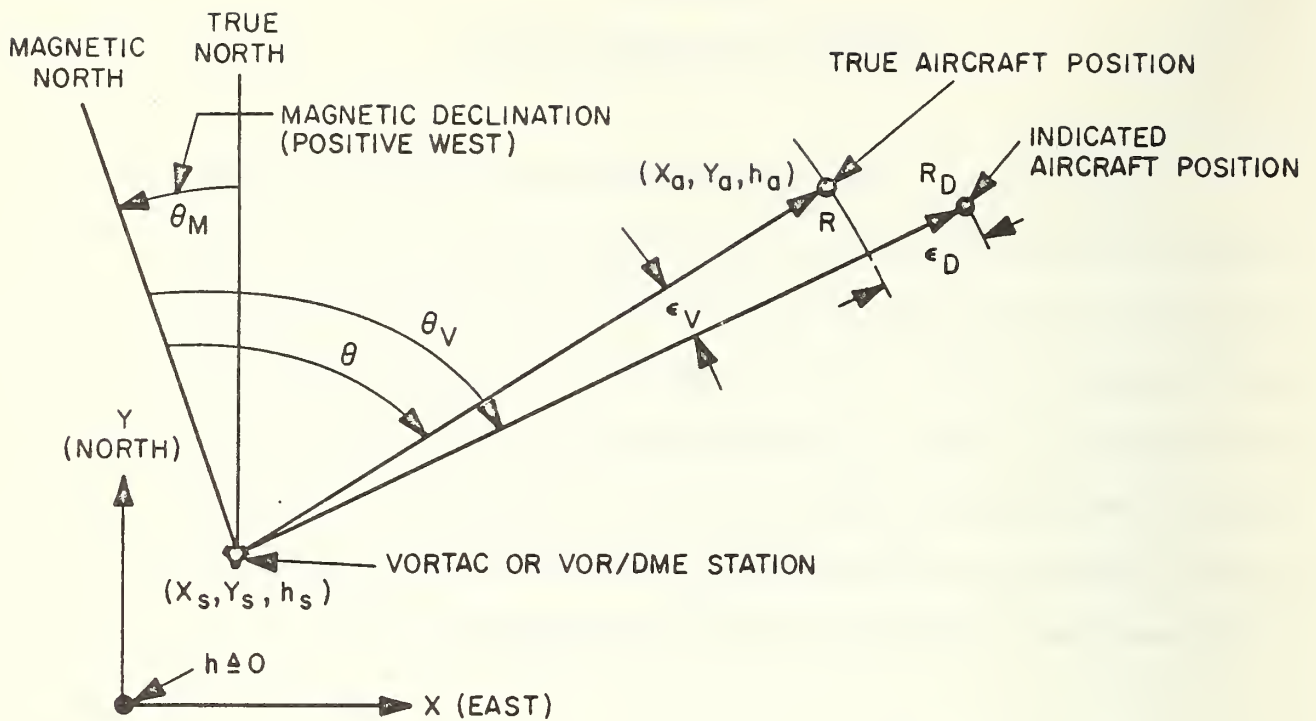
Figure 14. Geometry and Nomenclature for VOR/DME Model.

The indicated VOR bearing is in error by the amount ϵ_V:

$$\theta_V = \theta + \epsilon_V \tag{23}$$

where the total error includes receiver and transmitter biases and a course roughness error:

$$\epsilon_V = \epsilon_R + \epsilon_T + \epsilon_c \tag{24}$$

For each aircraft, ϵ_R is a random constant, selected from a normal distribution with zero mean and a standard deviation σ_R, i.e.:

$$\epsilon_R = N[0, \sigma_R] \tag{25}$$

Values of σ_R for high quality receivers are approximately 0.3° (Ref. 28) to 0.6°

- 40 -

(Ref. 30) with 0.2° claimed as possible for future ARINC equipment (Ref. 31).

Typical values of σ_R for average receivers seem to be about 1.0° to 1.5° (Refs. 10, 14, 24, 27).

ϵ_T is also a random constant for each VOR station:

$$\epsilon_T = N[0, \sigma_T] \tag{26}$$

For conventional VOR (CVOR) stations, σ_T is typically around 0.35° to 1.0° (Refs. 10, 14, 23, 24, 28 – 30). For doppler VOR (DVOR) transmitters σ_T is about 0.05° to 0.25° (Refs. 14, 24, 27, 32). Suggested values are 0.9° for CVOR and 0.15° for DVOR.

The position-dependent course roughness error is modeled as colored noise whose correlation time is inversely proportional to aircraft groundspeed, i.e.

$$\mathcal{E}[\epsilon_c(t)\epsilon_c(t + \tau)] = \sigma_c^2 e^{-\omega_c V_g |\tau|} \tag{27}$$

The standard deviation σ_c is approximately 0.9° for CVOR, 0.35° for DVOR and 0.2° for precision DVOR (Refs. 24, 28, 32, 33). The course roughness frequency is estimated between 0.2 and 2.0×10^{-3} rad/sec/kt for CVOR and about 4×10^{-3} rad/sec/kt for DVOR (Ref. 28). A suggested value for CVOR is 1×10^{-3} rad/sec/kt.

The course roughness error is generated from Gaussian white noise as shown in Figure 15. The autocorrelation function of the driving white noise is

$$\mathcal{E}[w_V(t)w_V(t + \tau)] = (2\sigma_c^2/\omega_c V_g)\delta(\tau) \tag{28}$$

The VOR model could be simplified by ignoring the magnetic variation θ_M and using true bearing as the measured quantity. If this is done, true heading instead of magnetic heading must be used for tracking a radial in the target dynamics
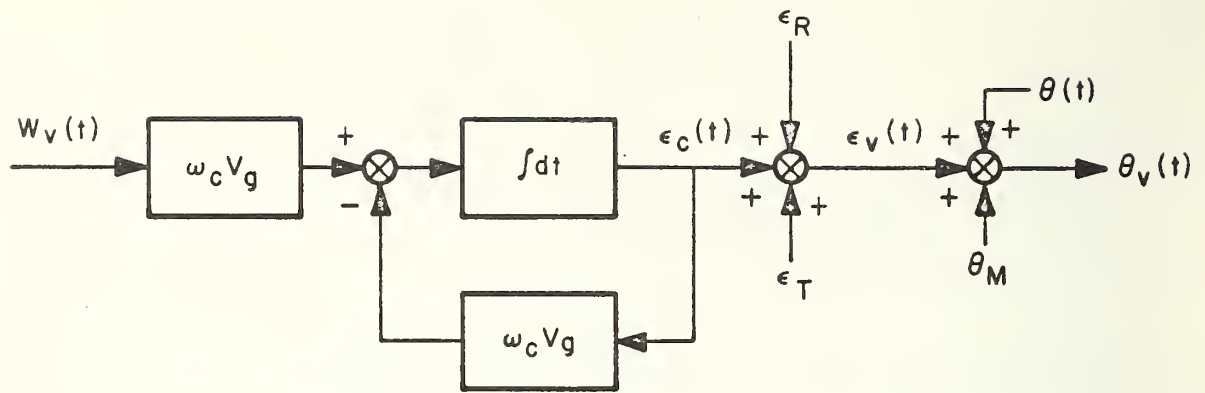
Figure 15. Block Diagram of VOR Error Model.

model. Thus it would not be necessary to maintain a continuous indication of θ_M at each aircraft's position.

The frequency of the VOR course roughness error model is independent of aircraft position or heading. This is not strictly accurate, but it does provide a substantially simpler model. In actuality, the course roughness for a specific VOR is definitely position-related, since much of it is the result of signal attenuation and/or reflection by the local terrain, structures and nearby aircraft. For example, two aircraft following nearly the same path within a short period of time would probably experience very similar course roughness. Also, the course roughness frequency would generally be different when flying along radials and while orbiting the station, as well as vary with altitude. However, due to the limited amount of data and the uncertainty associated with it, the simpler model was chosen. A much more complex model and a large amount of empirical data would be necessary to simulate the range, bearing and altitude dependence of the course roughness at a particular VOR station.

DME Model

The true slant range in nm between the DME station and the aircraft is

$$R = \sqrt{(x_a - x_s)^2 + (y_a - y_s)^2 + [0.0001646(h_a - h_s)]^2} \tag{29}$$

where x and y are in nm and h is in ft. The slant range indicated by the DME equipment is in error by ϵ_D:

$$R_D = R + \epsilon_D \tag{30}$$

The slowly-varying DME range error is modelled as colored noise with a correlation time of several minutes:

$$\mathcal{E}[\epsilon_D(t)\epsilon_D(t + \tau)] = \sigma_D^2 e^{-|\tau|/T_D} \tag{31}$$

T_D estimates range between 300 sec and 600 sec (Refs. 25,34); 400 sec is recommended as a compromise value.

The standard deviation in ϵ_D includes independent contributions from the aircraft interrogator (σ_I) and the DME station transponder (σ_S):

$$\dot{\sigma}_D = \sqrt{\sigma_I^2 + \sigma_S^2} \tag{32}$$

σ_I estimates range from less than 0.1 nm to about 0.25 nm, while σ_S is typically between 0.03 nm and 0.1 nm (Refs. 14, 24, 28, 30, 35, 36). The overall DME error σ_D estimates range from 0.015 nm to 0.5 nm (Refs. 10, 26, 34, 37). The airlines' goal for σ_D is ± 83 ft (.014 nm) for all-weather landing operations (Ref. 38). The recommended value of σ_D for most operators is 0.1 nm.

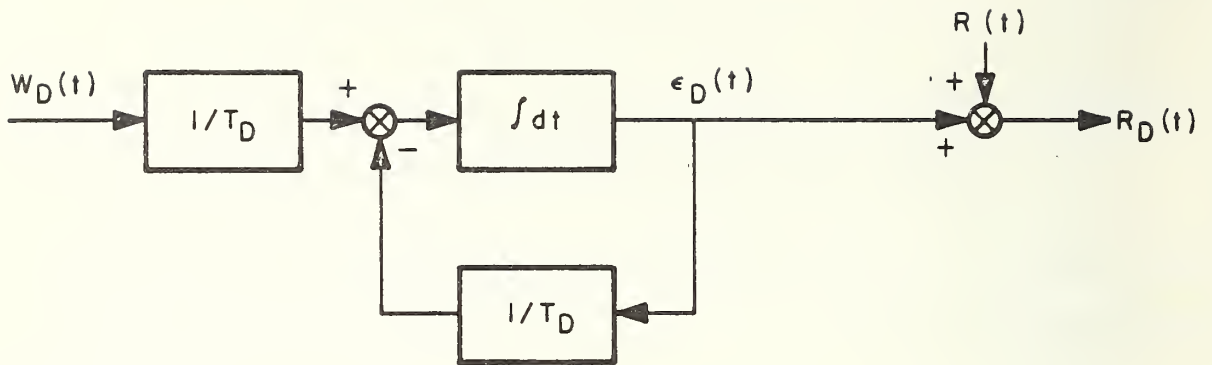As shown in Figure 16, the DME correlated error is generated from white noise with the autocorrelation function

Figure 16. Block Diagram of DME Error Model.

$$\mathcal{E}[w_D(t)w_D(t + \tau)] = 2\sigma_D T_d \delta(\tau) \tag{33}$$

Because the DME error is colored noise with a long correlation time, it could be closely approximated as a constant bias rather than a slowly-varying bias. This would substantially reduce the computation time for the model. Further justifications for this simplification are that the DME error is generally much smaller than the VOR error, and that very little information exists on the correlation time of the error.

Limits (Fig. 17)

The VOR and DME signals are both limited to line-of-sight to the station. Assuming a circular earth, this restricts the aircraft altitude to approximately:

$$h_a \geq \left[0.788 \sqrt{(x_a - x_s)^2 + (y_a - y_s)^2} - \sqrt{h_s}\right]^2 \tag{34}$$

For adequate VOR or DME signals, the slant range must be within a maximum value, $R \leq R_{max}$. For VOR's, R_{max} is determined to insure freedom of interference

- 44 -
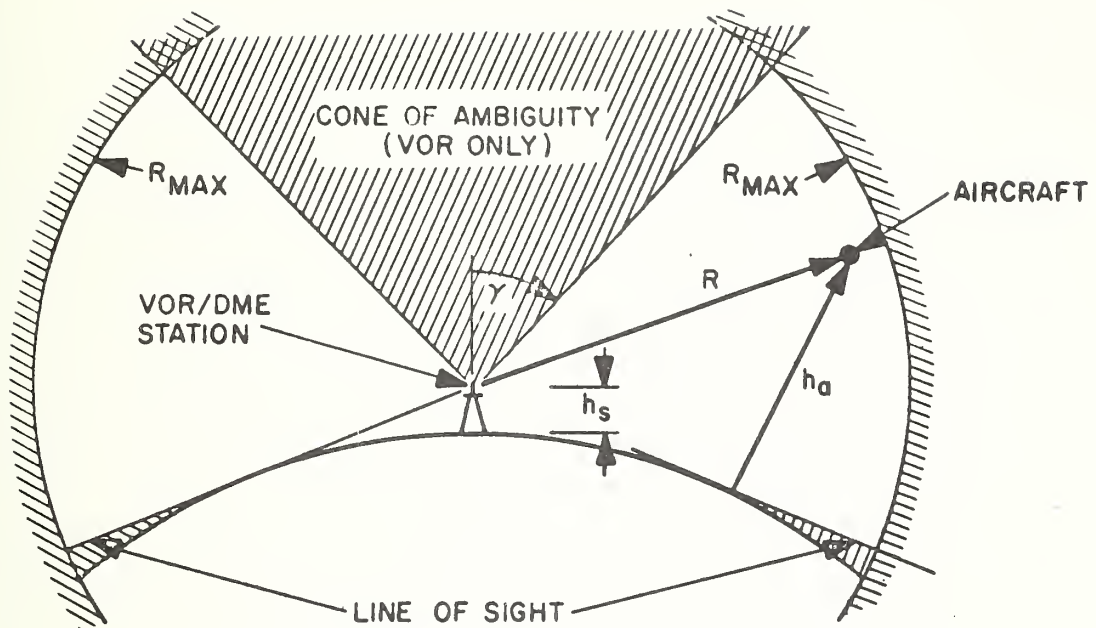
Figure 17. VOR/DME Limits.

by another station transmitting on the same frequency. For high altitude class
VORs, R_{max} is 130 nm (Ref. 39). The maximum ranges of most DMEs vary from
100 to 300 nm (Refs. 14, 26). ARINC 568 (Ref. 38) specifies a maximum error
of 0.2 nm at a range of 380 nm for future airline equipment.

For a usable VOR signal, the aircraft must be outside the cone of ambiguity
over the station. This limits the altitude to

$$h_a \leq h_s + 6,076.1 \sqrt{(x_a - x_s)^2 + (y_a - y_s)^2} \cot \gamma \qquad (35)$$

where the half-cone angle γ is typically between 15° and 30° (Refs. 23, 28, 31).

An alternative to explicitly including the limits in the model is for the
model user to include them implicitly. Under this approach, the user could apply
the model within the region of validity, or would use the limitations to interpret

- 45 -

his results. This could reduce the computation time slightly by avoiding the three checks every update.

5.2   AREA NAVIGATION SYSTEMS

Although the VOR/DME system provides nearly complete coverage of US airspace, available routes are limited by the requirement to fly from station to station. This has several disadvantages: the indirect routes are longer, much of the airspace is wasted, and the danger of collision is increased near the station where numerous airways converge. The use of area navigation (RNAV) equipment can alleviate these problems by permitting direct point-to-point navigation.

RNAV devices have been under development for many years, but only within the past half-decade has serious testing demonstrated the feasibility of area navigation (Refs. 25, 40). Since then, considerable progress has been made not only in the equipment itself, but in the development of standards and procedures for the implementation of RNAV in the National Airspace System (Refs. 41 - 45)

The RNAV system computer uses standard VOR/DME information to determine the aircraft's position relative to any course selected by the pilot. There are two forms of output. The more common output is range and bearing to a waypoint which has been established by a radial and distance from a given VOR/DME station. The second form of output is a linear display which shows the aircraft position relative to some map coordinates. The former approach has been selected for the VOR/DME RNAV model, while the latter will be used for the DME/DME RNAV model.

VOR/DME RNAV Model

Most available RNAV systems use the information from a single VOR/DME station for navigation. The RNAV routes are normally specified by waypoints, which

are defined by their bearing and distance from a given VOR/DME station. These way-points are treated as conveniently-located phantom VOR/DME stations, and then used for navigation in the normal fashion.

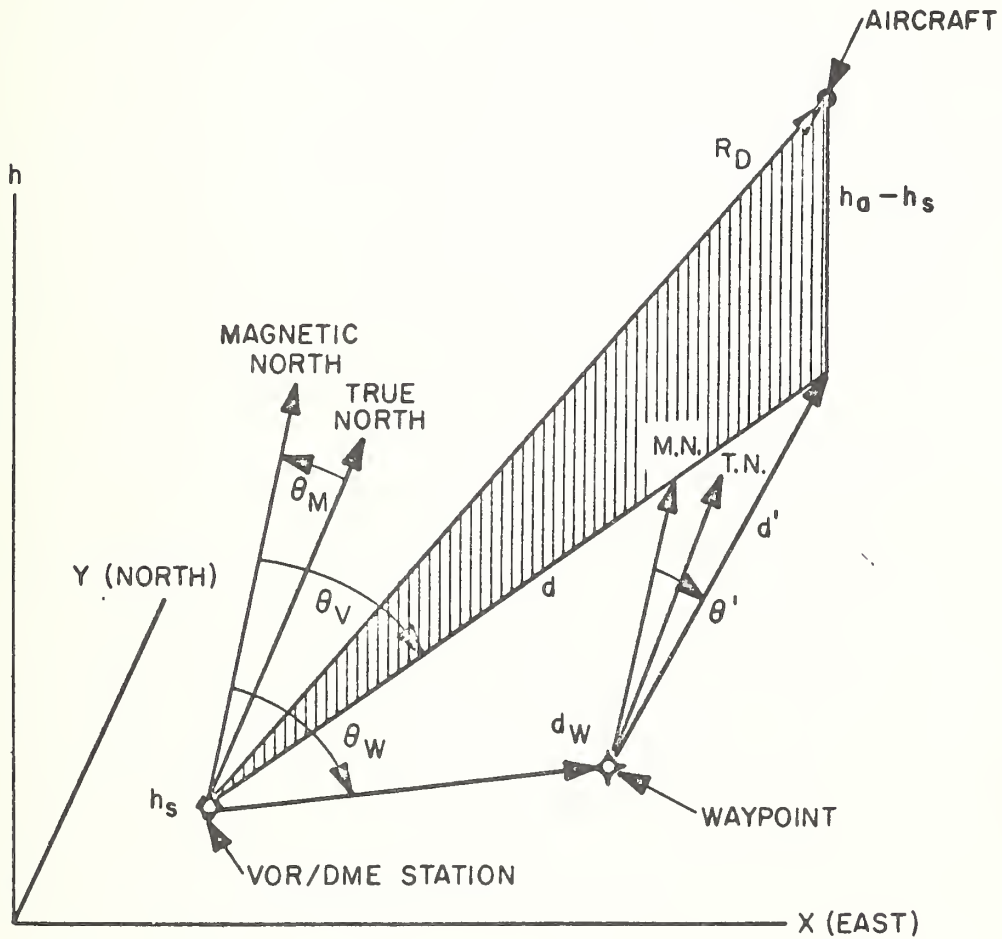Figure 18 illustrates the nomenclature and geometry used for the VOR/DME

Figure 18. Geometry and Nomenclature for VOR/DME RNAV Model.

RNAV model. The DME indicated slant range from the station to the aircraft is corrected for altitude

$$d = \sqrt{R_D{}^2 - [0.0001646(h_a - h_s)]^2} \qquad (36)$$

Slant range correction is normal but not universal in existing RNAV equipment. The FAA intends future rule-making to require it. Until then, RNAV airways will maintain sufficient separation from VOR/DME stations so that the slant range correction is negligible. RNAV approach procedures which require slant range correction will be limited to those aircraft which are so equipped.

The distance and bearing from the waypoint to the aircraft are found geometrically

$$d' = \sqrt{d^2 + d_w{}^2 - 2dd_w \cos(\theta_w - \theta_V)} \qquad (37)$$

$$\theta' = \theta_w - \sin^{-1}\left[\frac{d}{d'}\sin(\theta_w - \theta_V)\right] \qquad (38)$$

No error is included for the RNAV computations other than what exists for the VOR/DME sensors. In the less expensive systems there might be some computational error to be added. However, the more sophisticated RNAV systems would have reduced total error because of optimum filtering with air data or inertial measurements.

If the VOR/DME limits are included in the model, the RNAV inputs may be lost, for example, when flying through the VOR cone of ambiguity. If other navigation information is not provided to the RNAV system, this problem can be alleviated by continuously estimating groundspeed from position differences until the signal is lost, and then extrapolating the position until reacquisition of signal. Alternatively, the steering logic in the target dynamics model would maintain a constant heading during signal loss.

DME/DME RNAV Model

Instead of using range and bearing from a single VOR/DME station, the RNAV computer could use range or bearing information from two separate stations. Because the DME position error is generally much smaller than the VOR position error, the use of two DME's could theoretically provide much higher accuracy than two VOR's or a single VOR/DME.

The DME/DME RNAV model described below does not represent any known existing or proposed system. However, the model does provide an indication of the possible accuracy of a range-range-altitude navigation system. The DME/DME RNAV model geometry is illustrated in Figure 19. The two indicated DME slant ranges are corrected for altitude
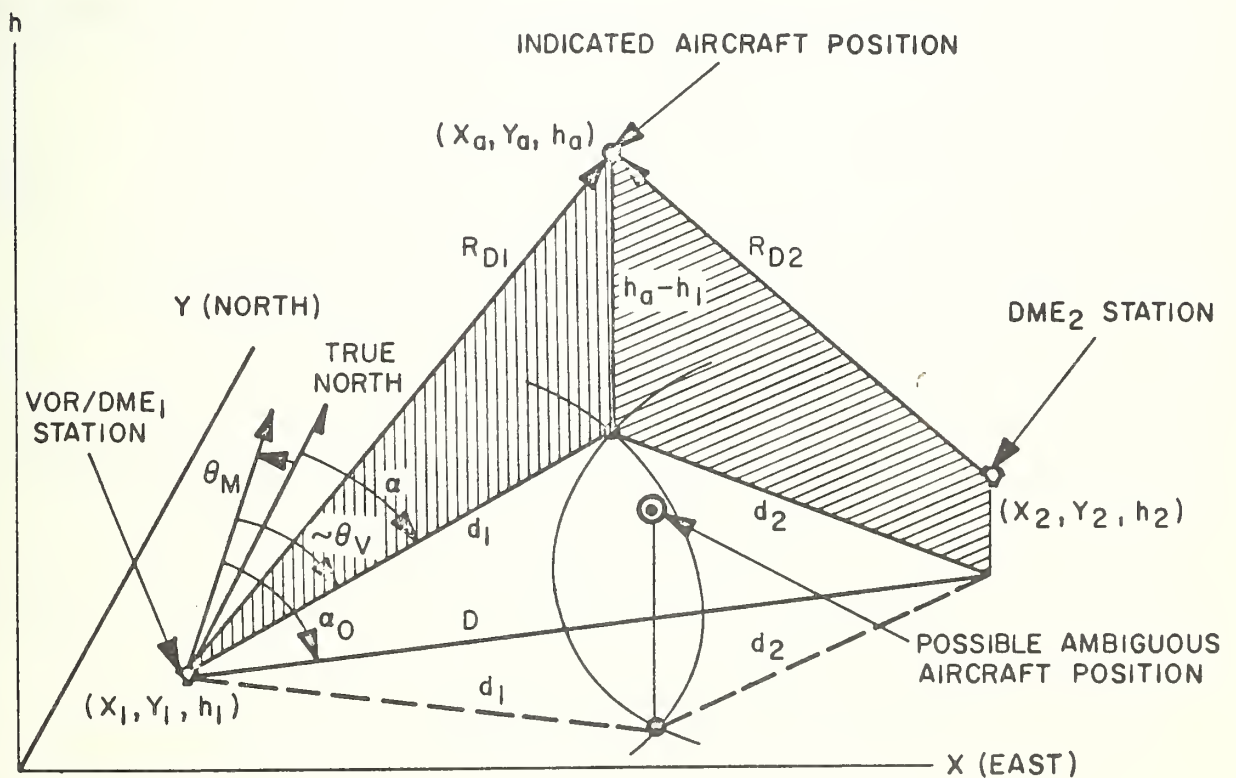

Figure 19. Geometry and Nomenclature for DME/DME RNAV Model.

- 49 -

$$d_1 = \sqrt{R_{D1}^2 - [0.0001646(h_a - h_1)]^2} \tag{39a}$$

$$d_2 = \sqrt{R_{D2}^2 - [0.0001646(h_a - h_2)]^2} \tag{39b}$$

The baseline horizontal distance between the two DME stations is

$$D = \sqrt{(x_2 - x_1)^2 + (y_2 - y_1)^2} \tag{40}$$

The location of the aircraft is determined from the intersection of the two horizontal circles of radii d_1 and d_2, centered at stations 1 and 2, respectively. Except for the special case $d_1 + d_2 \leq D$, there are two possible solutions for the aircraft position. To resolve this ambiguity, the bearing information from one of the stations (DME$_1$) is used.

The true bearing of the indicated aircraft position from the VOR/DME$_1$ station is found by geometry:

$$\alpha = \alpha_0 \pm \cos^{-1}[(D^2 + d_1{}^2 - d_2{}^2)/2d_1 D] \tag{41}$$

where α_0 is the true bearing from the VOR/DME$_1$ station to the DME$_2$ station:

$$\alpha_0 = \tan^{-1}(x_2 - x_1)/(y_2 - y_1) \tag{42}$$

Since $\theta_V - \theta_M \approx \alpha$, the choice of the sign in Equation (41) is determined as follows

$$\theta_V - \theta_M \begin{cases} \leq \alpha_0 \rightarrow \text{negative sign} \\ \\ \leq \alpha_0 \rightarrow \text{positive sign} \end{cases} \tag{43}$$

Finally, the indicated position components are found:

$$x_a = x_1 + d_1 \sin\alpha \tag{44a}$$

$$y_a = y_1 + d_1 \cos\alpha \tag{44b}$$

The VOR bearing data is used in this model only to resolve the ambiguity of position. However, the redundant information provided could be used with an optimal filter to provide somewhat better accuracy. Likewise, redundant data from other navaids, inertial systems and the air data system can be filtered together for improved performance (Refs. 34, 35, 46, 47).

Another drawback of DME/DME navigation is the high expense of the airborne equipment, in comparison to VOR equipment. A single airborne set could be switched between two or more ground stations, but this would introduce time delays for search and lock-on of each station, as well as the switching complexity.

SECTION 6

SURVEILLANCE SYSTEM MODEL

The present ATC system uses a dual network of radar systems to identify and track aircraft: The primary system uses pulsed-type search radar; the secondary system uses pulsed interrogators and airborne transponders to enhance the return pulses and identify the targets. Long range (200 nm) air route surveillance radars (ARSR) supply radar data for en route control, and separate shorter range (60 nm) airport surveillance radars (ASR) supply radar data in the critical terminal area. Table 2 summarizes the important parameters of the two systems (Ref. 10). Computer

Table 2. Present FAA Radar System Parameters.

Parameters	Terminal Radar	En Route Radar
Max range	60 nm	200 nm
Elevation coverage	0° to 30°	0° to 30°
Fan beam azimuth bandwidth	1.5°	1.35°
Frequency	2700 to 2900 MHz	1280 to 1350 MHz
Scan Rate (continuous)	15 rpm	6 rpm
PRF* (nominal)	1200 pps	360 pps
Pulse width	0.833 μsec	1.95 μsec

*Pulse Repetition Frequency

processing of the radar surveillance information provides easy transfer and accurate

processing and updating of flight information, aids for establishing and maintaining radar identification of aircraft, and automatic display of altitude and groundspeed information with aircraft track position.

Control of IFR traffic is based primarily on use of the ATC radar beacon system (ATCRBS) replies for surveillance. Primary radar data is available for tracking unequipped aircraft and for airborne transponder failures. Satellite surveillance systems are presently being investigated for future ATC applications, particularly over oceanic routes.

6.1   GROUND SURVEILLANCE

The ground surveillance model described below is based on the ATCRBS in the Third Generation air traffic control system. The geometry and nomenclature for the ground surveillance model is shown in Figure 20. During each scan the
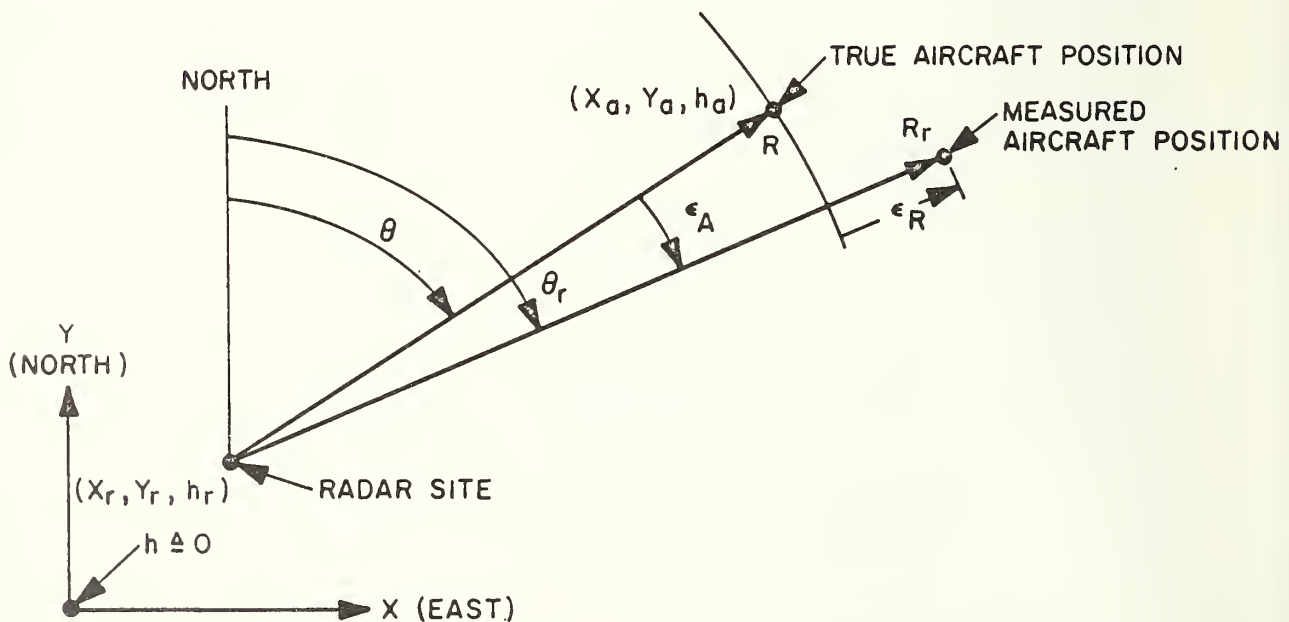

Figure 20. Ground Surveillance Geometry and Nomenclature.

transponder will be interrogated several times as the radar beam sweeps across the aircraft. The beacon processor records the azimuth and range of each successful beam reply (hit). The range and azimuth of each hit are quantized and entered in a two-dimensional table of range-azimuth cells, as illustrated in Figure 21.
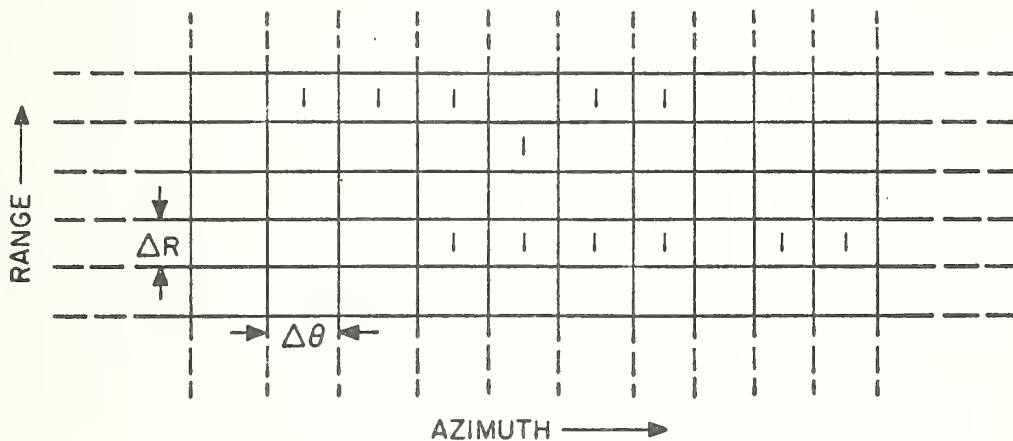

Figure 21. Range-Azimuth Cells in Beacon Target Processor.

A "1" in the figure indicates a hit was detected with a range between R and R + ΔR, and with an azimuth between θ and θ + $\Delta\theta$. In the terminal area, the range bin ΔR is 1/16 nm, and the azimuth bin $\Delta\theta$ is $0.088°$. The corresponding values for the en route system are 1/4 nm and $0.225°$. Based on certain statistical criteria, a target detection algorithm scans all hits at a given range to declare a beacon target and to establish its leading and trailing edges (Ref. 48). The azimuth center mark of the target is determined by averaging the leading and trailing edge positions and adding a bias which is a function of the target detection parameters.

The true azimuth from the radar to the aircraft is (Fig. 19):

$$\theta(t_i) = \tan^{-1}[(x_a - x_r)/(y_a - y_r)] \tag{45}$$

The observation times t_i are $t_i = 0, T, 2T, 3T$, etc. The radar scan period in

- 55 -

seconds is

$$T = 60/\Omega \tag{46}$$

where Ω is the radar scan rate in rpm.

The radar azimuth error ϵ_A includes the effects of interrogator and transponder errors and the quantization error in the beacon target processor. The error is modeled by assuming the unquantized error on each scan ϵ_A' is a normally-distributed random variable with zero mean and standard deviation σ_A:

$$\epsilon_A' = N[0, \sigma_A] \tag{47}$$

σ_A is typically $0.25°$ to $0.4°$ for the terminal radar, with $0.12°$ possible; the slower scan rate of the enroute system reduces σ_A by a factor of about 2.5 (Refs. 10, 49, 50). The indicated radar azimuth neglecting the quantization error is given by

$$\theta_r'(t_i) = \theta(t_i) + \epsilon_A'(t_i) \tag{48}$$

This value is quantized to the azimuth bin size to obtain the final indicated azimuth:

$$\theta_r(t_i) = n \, \Delta\theta \tag{49a}$$

where n is found such that

$$n \, \Delta\theta \leq \theta_r'(t_i) < (n + 1) \, \Delta\theta \tag{49b}$$

The true range in nautical miles from the radar to the aircraft is

$$R(t_i) = \sqrt{(x_a - x_r)^2 + (y_a - y_r)^2 + [0.0001646 \, (h_a - h_r)^2]} \tag{50}$$

where x and y are in nm and h is in ft. The indicated radar range each scan is in error by an amount ϵ_R due to the quantization effect and to inaccuracies in

- 56 -

the elapsed time between interrogation and reply. The primary factor in the range
measurement error is a bias due to lack of precise delay control in the aircraft
transponder system. Therefore the range measurement error neglecting quantization
ϵ'_R is modeled as a random bias, constant for each aircraft, which is selected
from a normal distribution with zero mean and standard deviation σ_R:

$$\epsilon'_R = N[0, \sigma_R] \tag{51}$$

Estimates of σ_R are typically 1/32 to 1/16 nm (190 ft to 380 ft), with 100 ft possible
with tightened equipment specifications (Refs. 10, 49, 50). The indicated radar
range neglecting the quantization error is given by

$$R'_r(t_i) = R(t_i) + \epsilon_R \tag{52}$$

This value is quantized to the range bin size, to obtain the final indicated value

$$R_r(t_i) = m \, \Delta R \tag{53a}$$

where m is found such that

$$m \, \Delta R \le R'_r(t_i) < (m + 1) \, \Delta R \tag{53b}$$

A possibly significant phenomenon of the ATCRBS is the probability of
lost replies. These may be caused by 1) overinterrogation by many interrogators
which cause dead time in the transponders, or decrease their sensitivity; 2) poor
coverage produced by interrogator siting limitations and/or multipath nulls; and
3) aircraft antenna shielding, particularly during turning maneuvers. Dropout
due to aircraft banking is the most important effect for the simulation since the
probability of a dropout is two or three orders of magnitude higher, and the dropout
is likely to continue over several scans. This can be represented in the model
by the following procedure:

1. Test the aircraft turn rate for a maneuver. A suggested criterion is a turn rate magnitude of 2 deg/sec or greater.

2. If the maneuver test is positive, generate a random number from a uniform distribution between 0 and 1. A lost reply is assumed if this number is less than the specified probability for signal dropout. The probability of dropout during a turning maneuver is estimated to be about 0.05 to 0.10.

3. Once a particular target has suffered a dropout in step 2, increase its probability of dropout during the remainder of that maneuver to about 0.8 to 0.9.

The output of the ground surveillance model is shown as measured range and azimuth, which are converted to rectangular position coordinates in the radar tracking model. However, the conversion could occur in the ground surveillance model, in which case the inputs to the tracking model would be x_r and y_r.

The rotating characteristic of the surveillance antenna has not been included in the model, i.e, the measured positions and times do not depend upon the targets' relative azimuths from the antenna. Instead, the model provides a snapshot of all measured aircraft positions at the same time once each scan. This provides a substantial simplification in the model implementation, without significantly compromising its performance.

Limits (See Fig. 22)

Radar is subject to a maximum elevation angle γ_{max}, which restricts the altitude of the aircraft in the vicinity of the radar for a useful return;

$$h_a \leq h_r + 6,076.1 \sqrt{(x_a - x_r)^2 + (y_a - y_r)^2} \tan \gamma_{max} \tag{54}$$

The normal elevation angle limit is 30° for radar, and 45° for ATCRBS (Ref. 10).

For a usable return, the aircraft must be within line-of-sight of the radar antenna. For a circular earth, this implies

$$h_a \geq \left[0.788 \sqrt{(x_a - x_r)^2 + (y_a - y_r)^2} - \sqrt{h_r} \right]^2 \tag{55}$$
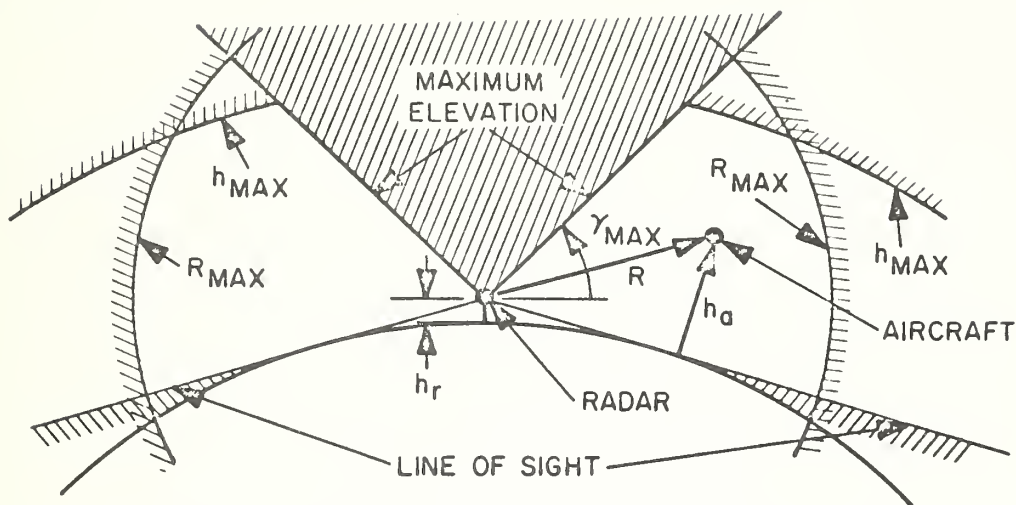
Figure 22. Ground Surveillance Model Limits.

The slant range between the aircraft and ground antenna must be less than R_{max} to ensure adequate signal strength of the return. R_{max} is about 60 nm for ASR, and around 200 nm for ARSR and ATCRBS. The radar may be subject to a maximum altitude restriction $h \leq h_{max}$. For ASR, h_{max} is specified as 10,000 ft.

Implementation of the model could be slightly simplified by not including the limits explicitly. In this case, the model user should be aware of the restrictions and make sure he does not violate them, or at least uses them to interpret his results correctly.

6.2 RADAR TRACKING

The radar tracker provides estimates at each scan of the target position and groundspeed based on the noisy radar data. The present ATC system uses an "$\alpha - \beta$ tracker" (Refs. 51. 52) which provides a weighted first-order correction to the position and groundspeed each scan. More sophisticated systems (Refs. 53 - 57)

- 59 -

have been investigated and could provide better tracking at the expense of more computation. Figure 23 defines important geometry and nomenclature for the $\alpha - \beta$ tracking model.

The measured slant range and azimuth of the target on scan i are resolved into approximate rectangular components:

$$x_i = x_r + R_{r_i} \sin \theta_{r_i} \tag{56a}$$

$$y_i = y_r + R_{r_i} \cos \theta_{r_i} \tag{56b}$$

The measured position coordinates then are used to correct the predicted position at t_i which was calculated on the previous scan:

$$\hat{x}_i = x_{p_i} + \alpha(x_i - x_{p_i}) \tag{57a}$$

$$\hat{y}_i = y_{p_i} + \alpha(y_i - y_{p_i}) \tag{57b}$$

The parameter α weights the contribution of the measurement to the updated position estimate.

The estimated groundspeed components from the previous scan are updated, for the current scan using x_i and y_i:

$$\hat{\dot{x}}_i = \hat{\dot{x}}_{i-1} + \frac{\beta}{T}(x_i - x_{p_i}) \tag{58a}$$

$$\hat{\dot{y}}_i = \hat{\dot{y}}_{i-1} + \frac{\beta}{T}(y_i - y_{p_i}) \tag{58b}$$

where, in the first scan of a new target, $\hat{\dot{x}}_0 = \hat{\dot{y}}_0 = 0$. β is a weighting parameter which determines how much the updated groundspeed changes. The estimated groundspeed in knots is computed as
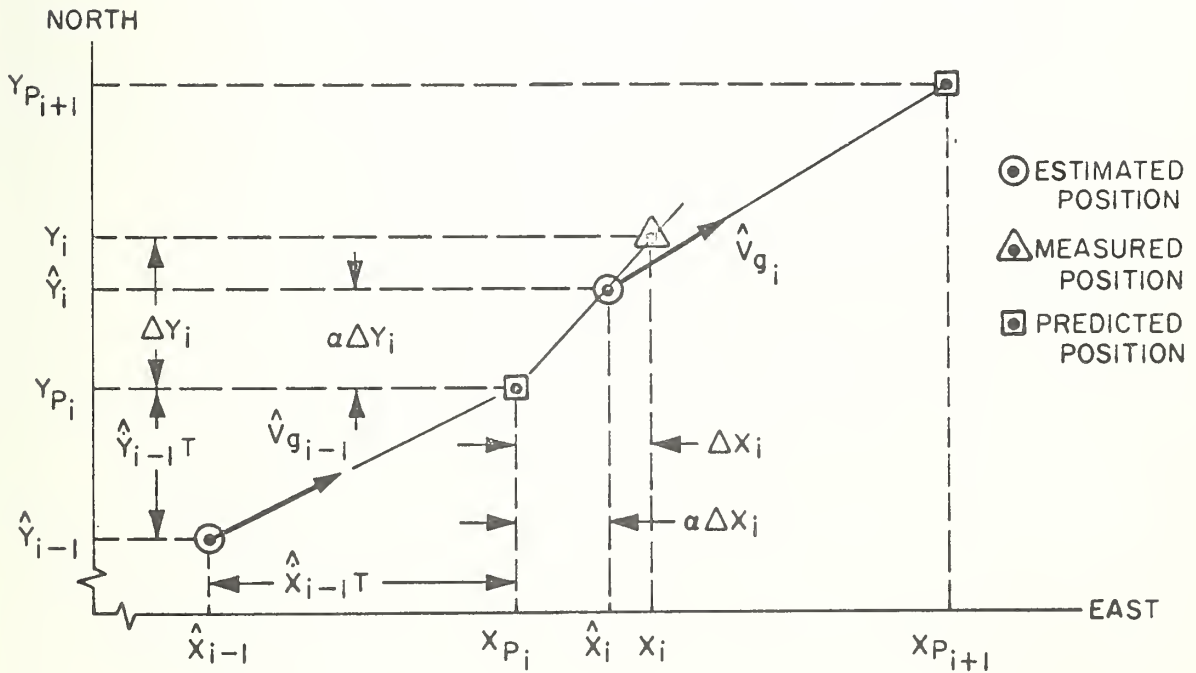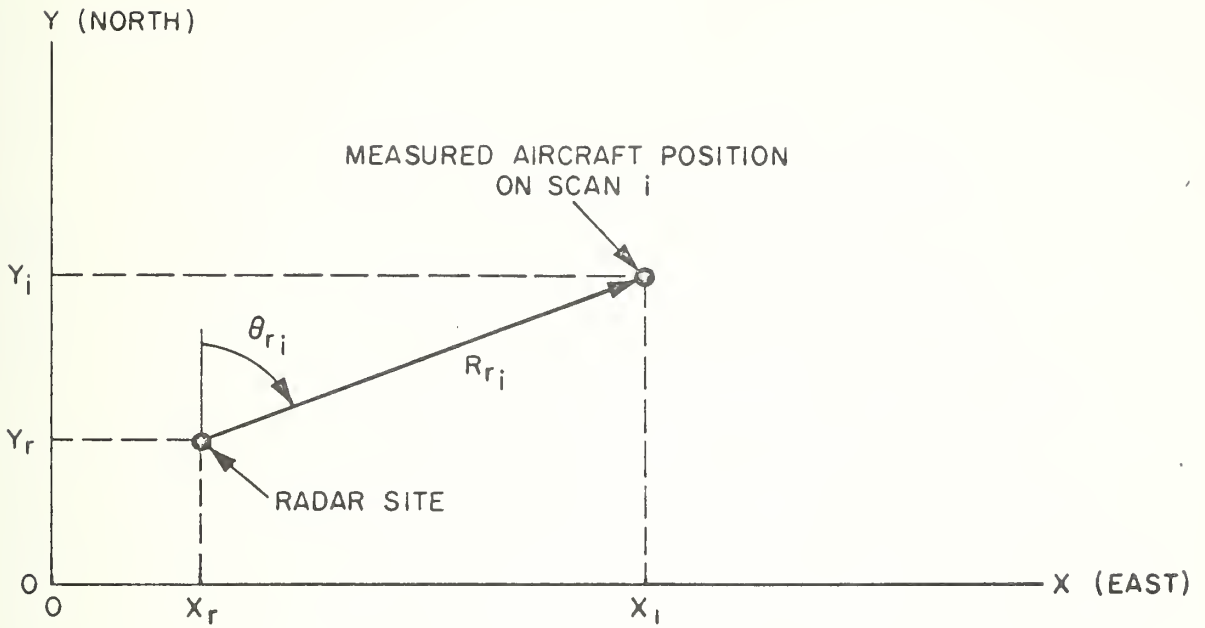
Figure 23. Radar Tracking Geometry and Nomenclature.

$$\hat{V}_{g_i} = 3600 \sqrt{\hat{\dot{x}}_i^2 + \hat{\dot{y}}_i^2} \tag{59}$$

The current estimated position and groundspeed components are then used to predict the aircraft position on the next scan:

$$x_{P_{i+1}} = \hat{x}_i + \hat{\dot{x}}_i T \tag{60a}$$

$$y_{P_{i+1}} = \hat{y}_i + \hat{\dot{y}}_i T \tag{60b}$$

As mentioned in the Ground Surveillance Model comments, the conversion from polar to rectangular coordinates could be performed in either model. This conversion has been included in the tracking model for two reasons:

a)   If Mode C (i.e. automatic altitude reporting) capability is available, the tracking computer can use the aircraft altitude to correct for slant range in converting to rectangular coordinates. At high elevation angles, the slant range can introduce position errors of more than 40%.

b)   In the ARTS III tracker, radar range and azimuth are used directly in correlating target returns with aircraft tracks. Thus, if a more detailed model of the ARTS III tracker is developed later, it will be compatible with the present models.

A major element of the ARTS III tracker (Ref. 58) is the correlation of beacon replies with active tracks. Because the beacon reply is frequently lost, garbled, reflected or duplicated, ARTS III includes an elaborate and complicated logic for correlation. The confidence level of the track's position is a function of the number of successful correlations. Whenever a track is not successfully correlated, its confidence level is decreased, and the estimated position is equated to its predicted position. On a successful correlation, the predicted position is updated by Equation (57) and the confidence level increased.

The magnitudes of the update parameters (α, β) are functions of the individual

track's confidence level: the higher the confidence level, the more weight is placed on its predicted position and the less on the new measurement (see Table 3).

Table 3. Variation of ARTS III Tracking-Parameters with Successful Correlation.

Scan	64α	64β
1	64	0
2	64	64
3	51	36
4	44	24
5	38	16
6	34	12
7	30	9
8	27	7
9	24	6
10	22	5
≥ 11	21	4

At the beginning of a track the position measurement is used entirely and ground-speed is not calculated. After the track has successfully correlated for 11 or more scans, the weighting parameters reach a steady-state condition. On an unsuccessful correlation, the sizes of the weighting parameters are increased slightly (about 1/2 step). The track is placed in a permanent coast mode and the controller alerted

after three successive unsuccessful correlations.

Two versions of the tracker could be implemented in the TSC simulation without requiring the very complex correlation logic in ARTS. The simpler tracker would use constant values of α and β; the steady-state values in Table 3 are recommended. A more accurate model would include the variation of α and β shown in Table 3. In the event of lost replies the track would be coasted, as discussed above, but α and β would remain at their previous values since the actual increases are very small.

The correlation and updating calculations of the tracker require a finite period of time to perform. In ARTS III, the position and groundspeed estimates are delayed by about one second after the surveillance measurements. This delay is probably not significant enough to warrant inclusion in the model.

As in the surveillance model, the effects of the relative azimuths of the targets are not included in the tracking model. The tracks are all updated at the same time each scan. This eliminates such complications as modifying the predicted position to account for a change in measurement time due to a change in azimuth.

SECTION 7

DISCUSSION

The models presented in the previous sections have been developed to provide more accuracy and realism for simulations requiring the high frequency response of advanced air traffic control systems. Addition of these models to the existing program will add greater realism to the simulation, but will also require more computer time. In general, the more sophisticated models should only be used when the simpler models are inadequate. The following discussion compares the results one would expect using the simple as opposed to the complex model and indicates when it would be desirable to use the more realistic model.

The ROSS simulation modeled the wind by layers of constant direction and velocity. Early in the present study it was recommended that a more reasonable model would provide a linear variation of both wind speed and direction with altitude. This suggestion has since been implemented in the simulation program. It was concluded the effects of vertical winds and higher frequency wind gusts would be much smaller than the other errors being modeled, and therefore unnecessary to include.

In the present program the airspeed does not change immediately with wind changes but the groundspeed does suddenly jump to its steady-state value. The real aircraft responds to sudden wind changes by having its airspeed suddenly change to the new steady-state value with the groundspeed eventually catching up, an effect which is included in the more sophisticated model. Normally the difference between the two models is insignificant because the pilot is using thrust to hold airspeed constant in a fairly tight control loop. The more sophisticated model would be desirable when one is using groundspeed instead of airspeed commands such as in 4-D guidance, or when there is concern about the effects of gusts or

severe wind shears.

Altitude in the present program is changed at a constant rate until it reaches its new value, where it stops abruptly. The new model uses two rates and makes the transition more realistic by including a response lag and by limiting the normal acceleration. The more sophisticated model would be desirable where altitude separations are critical, such as the evaluation of CAS or IPC. Figures 24 - 27 compare the altitude response models for four aircraft ranging from single-engine propeller to standard commercial jet. The ASI model results were obtained by digital simulation of the model described in Section 3.1, neglecting any air data system errors. In the revised (ASI) model, the rate of climb or descent decreases to 500 fpm when the altitude difference is less than 1,000 ft. Because of the altitude tolerance in the new model, the aircraft begins to level off when it is within 50 ft of the desired altitude. The simulation was stopped when the altitude difference was within 50 ft and the altitude rate was less than 50 fpm.

Airspeed changes in the present system are also at a constant rate until reaching the desired value. The new model introduces a time lag into the application of acceleration, and also limits acceleration during climb and deceleration during descent in accordance with physical reality. The more sophisticated model would be desirable particularly where velocity control is being used for separation, spacing or merging. Figures 28 - 31 compare the responses of the two models to commanded airspeed changes, simultaneously with the altitude changes shown in Figures 24 - 27. Again the ASI results were obtained by simulation, neglecting the air data system errors and assuming no winds. The simulation was terminated when the airspeed error was less than 2.5 kts and the acceleration (or deceleration) was within 10% of ACR (or DCR), and the altitude and altitude rate criteria above were satisfied simultaneously. The airspeed response of the present model is unaffected by the
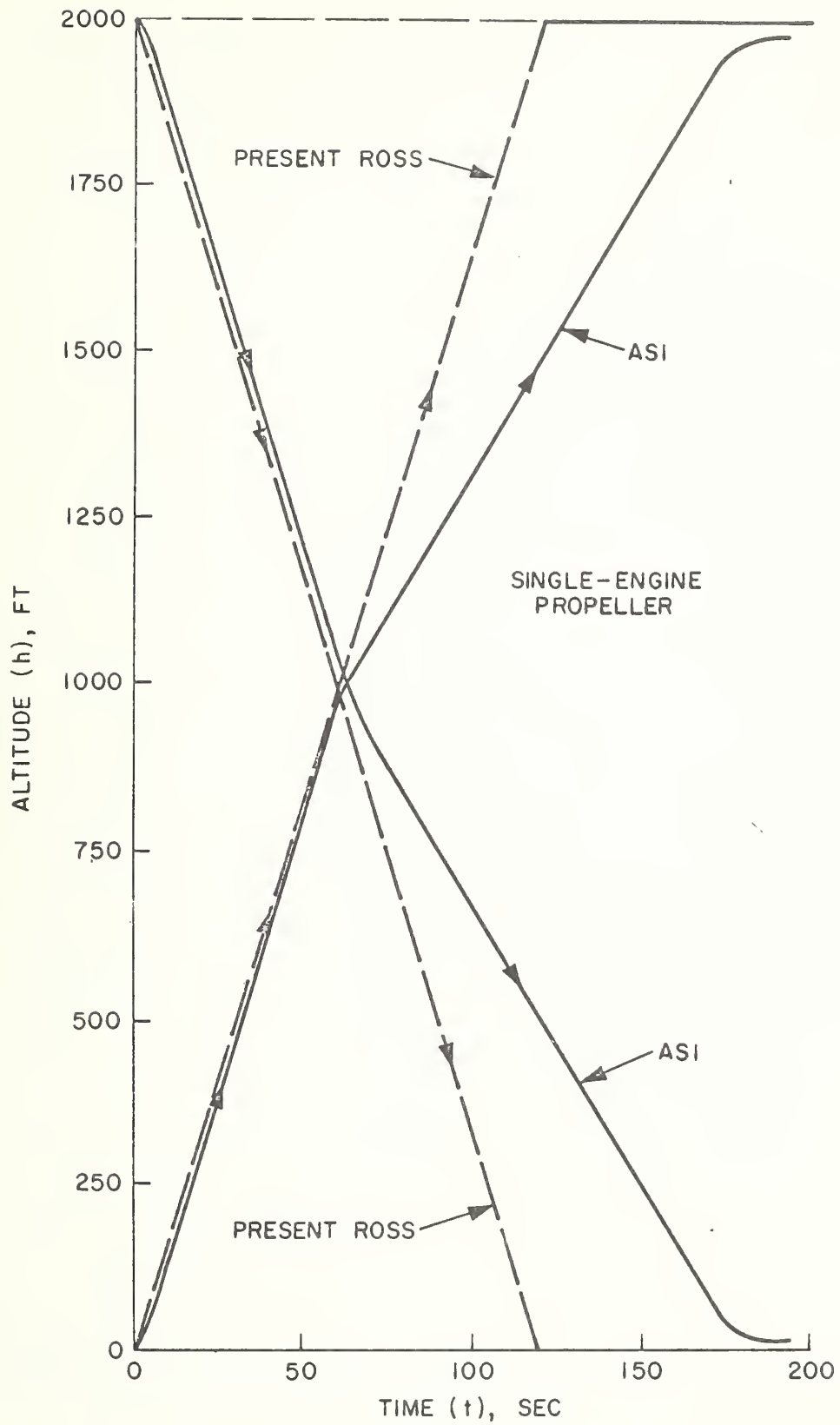
Figure 24. Comparison of ROSS and ASI Altitude Response Models for a Climb and a Descent (Single-Engine Propeller Aircraft).

Figure 25. Comparison of ROSS and ASI Altitude Response Models
for a Climb and a Descent (Medium Turbo-Prop Aircraft).
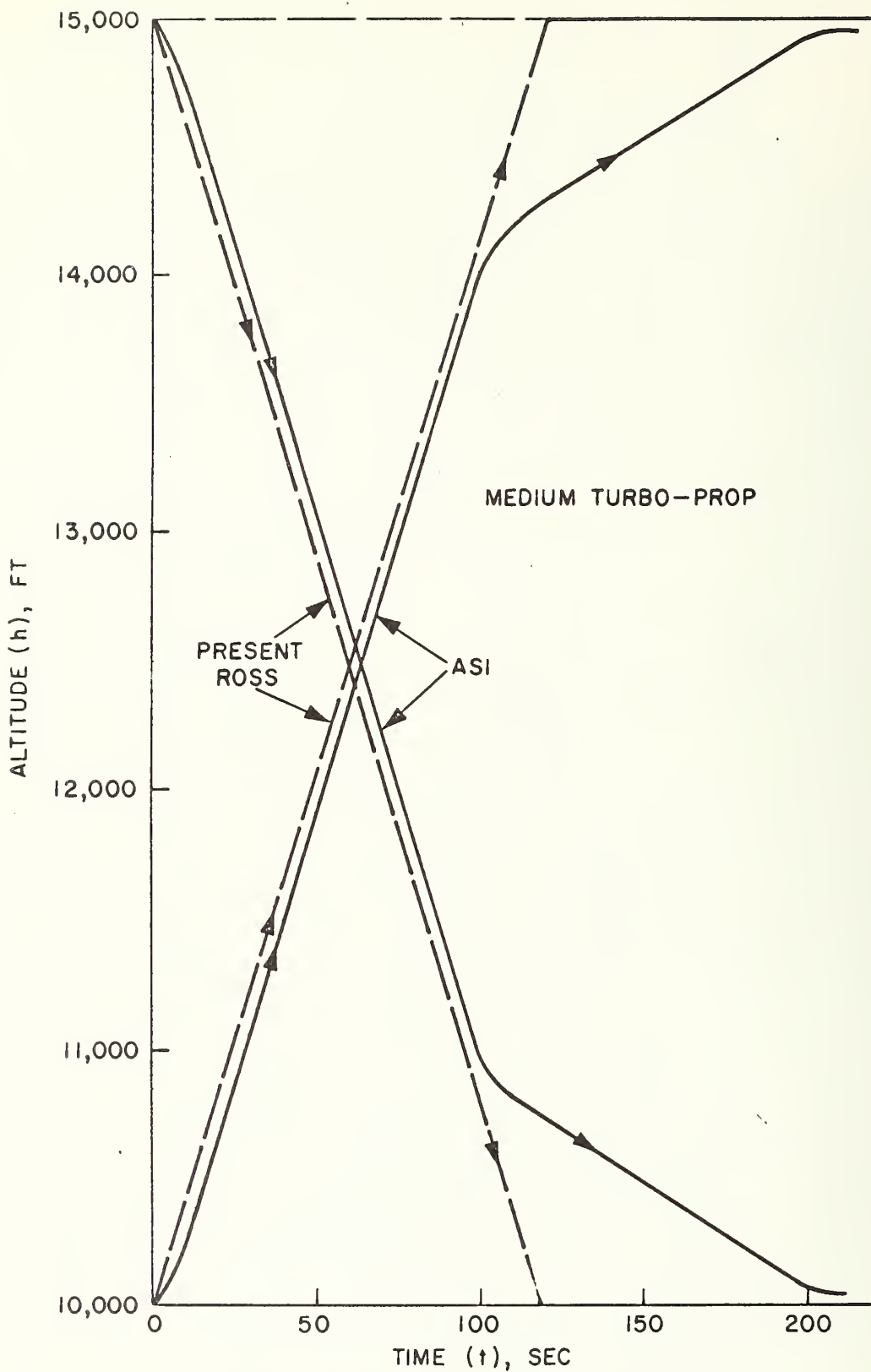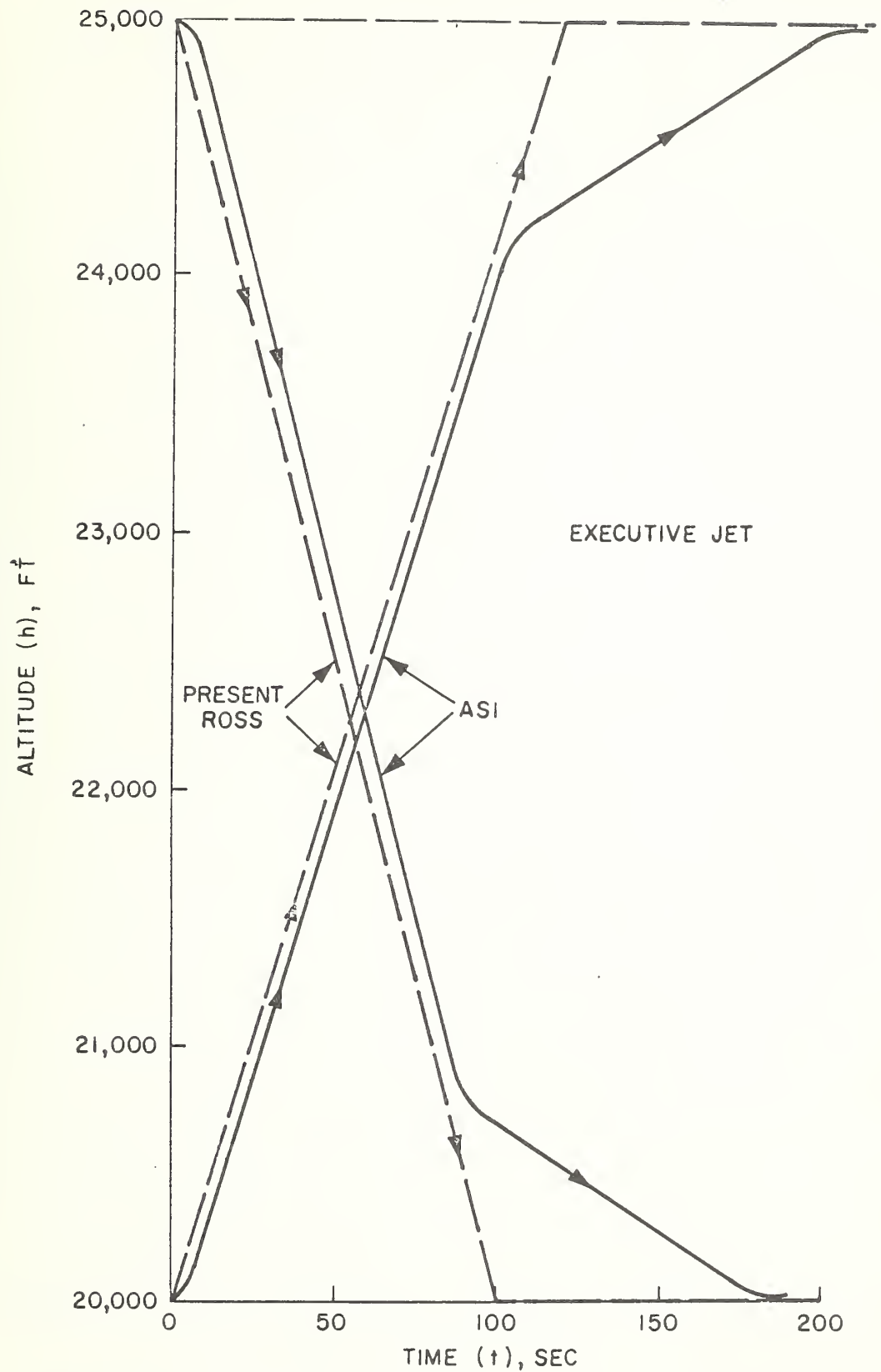
Figure 26. Comparison of ROSS and ASI Altitude Response Models
for a Climb and a Descent (Executive Jet Aircraft).
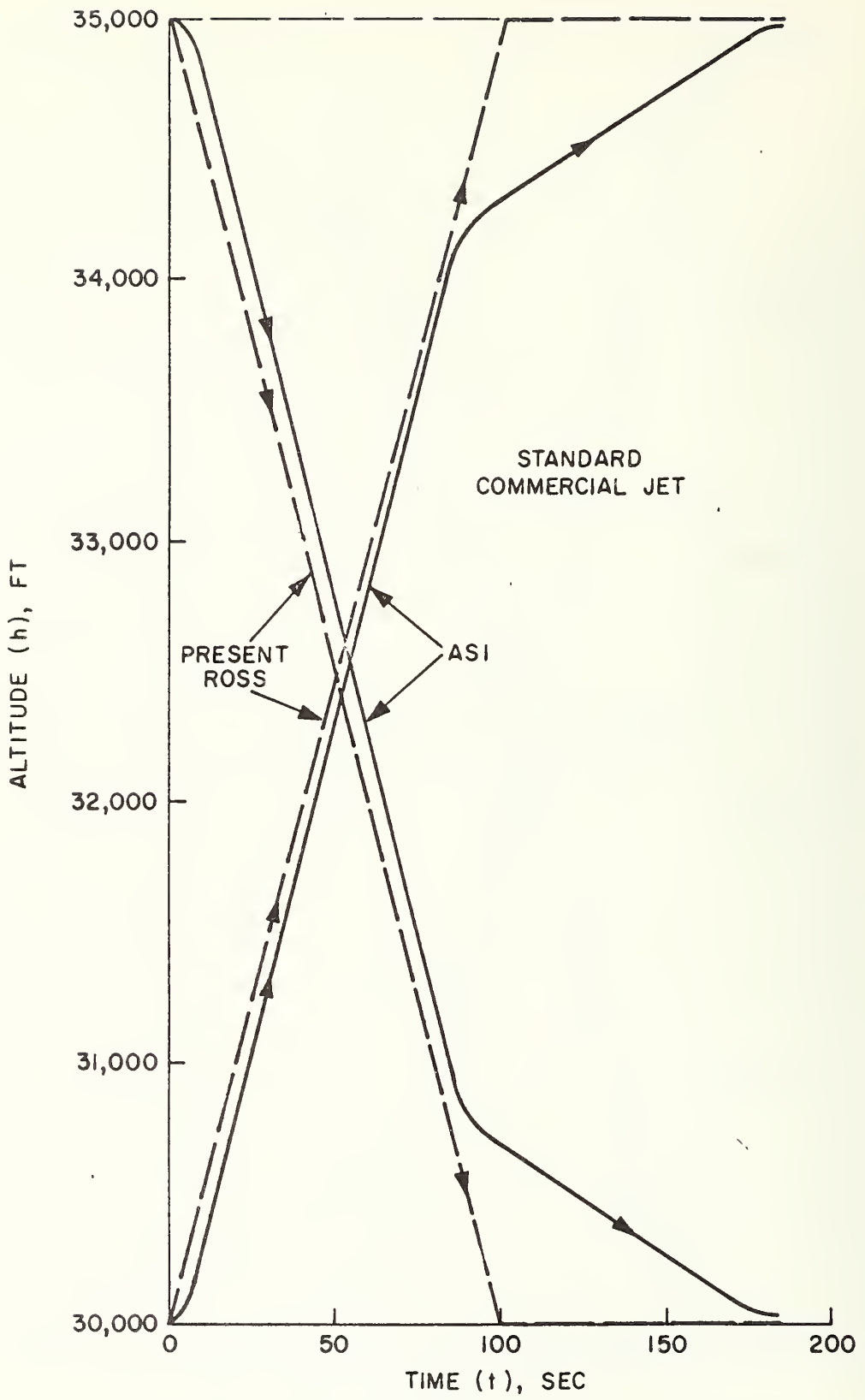
Figure 27. Comparison of ROSS and ASI Altitude Response Models for a Climb and a Descent (Standard Commercial Jet Aircraft).

Figure 28. Comparison of ROSS and ASI Velocity Response Models
for Climbing Speed-Up and Descending Slow-Down
(Single Engine Propeller Aircraft).

- 71 -

Figure 29. Comparison of ROSS and ASI Velocity Response Models
for Climbing Speed-Up and Descending Slow-Down
(Medium Turbo-Prop Aircraft).

Figure 30. Comparison of ROSS and ASI Velocity Response Models
for Climbing Speed-Up and Descending Slow-Down
(Executive Jet Aircraft).

- 73 -
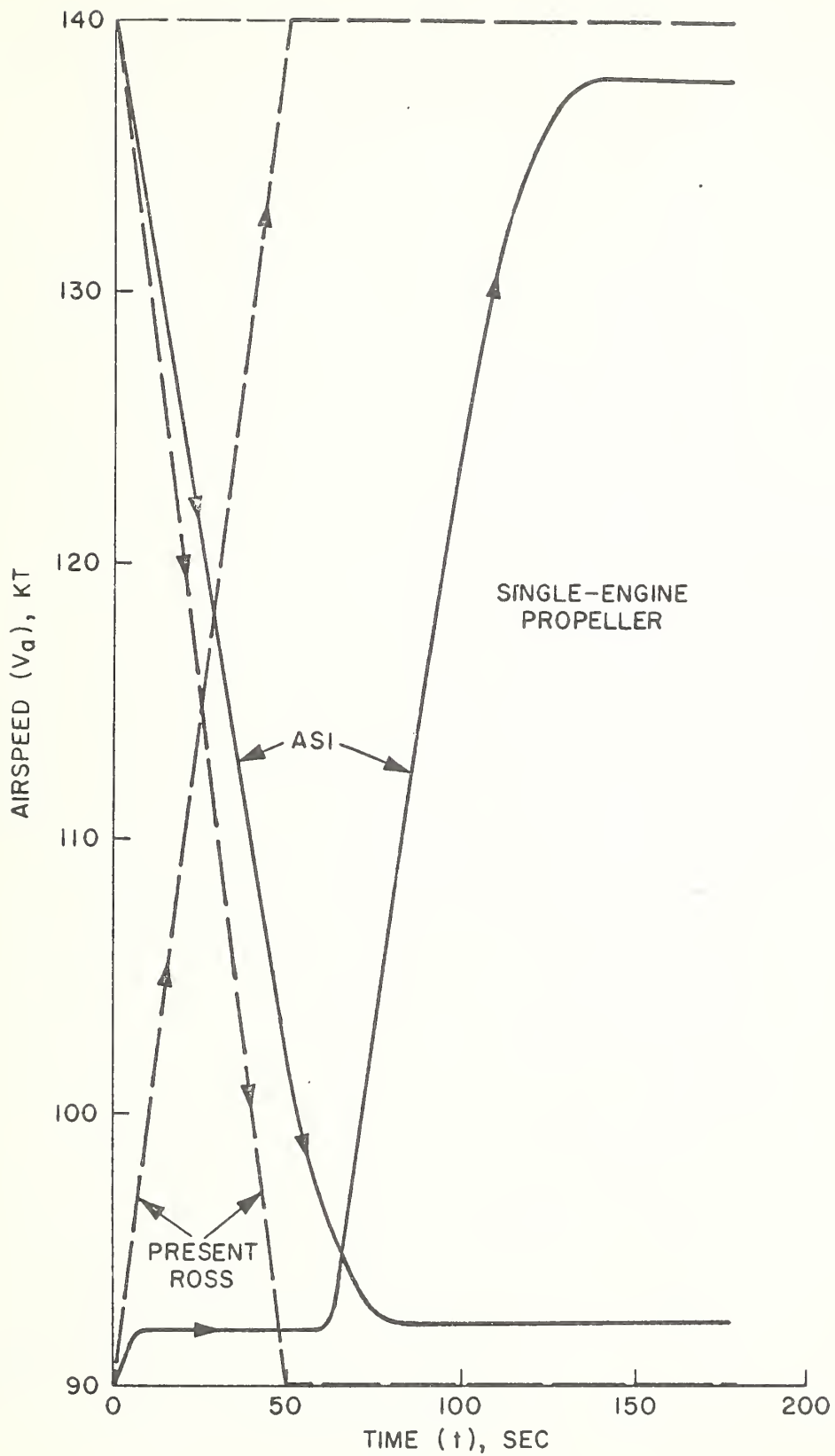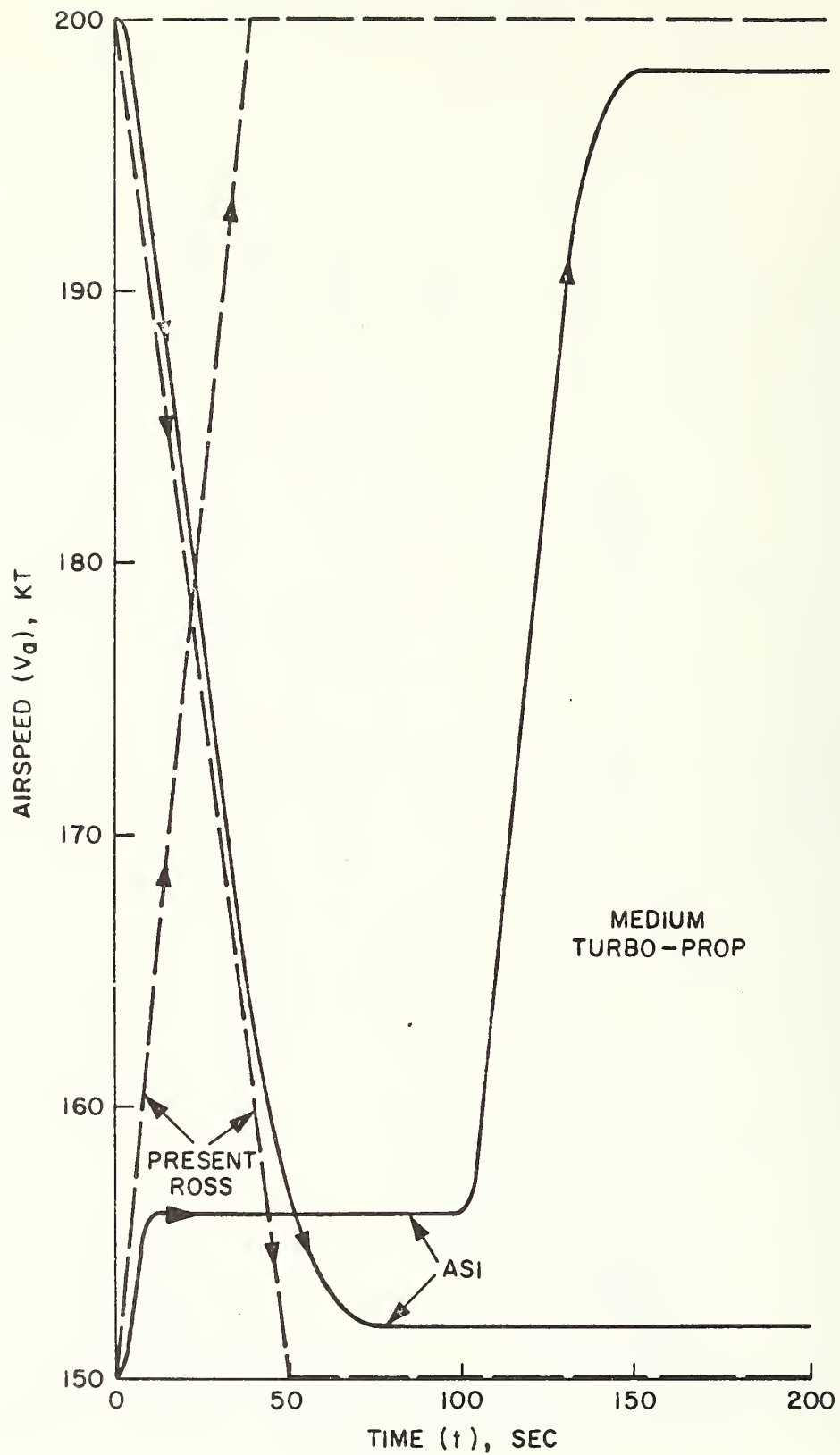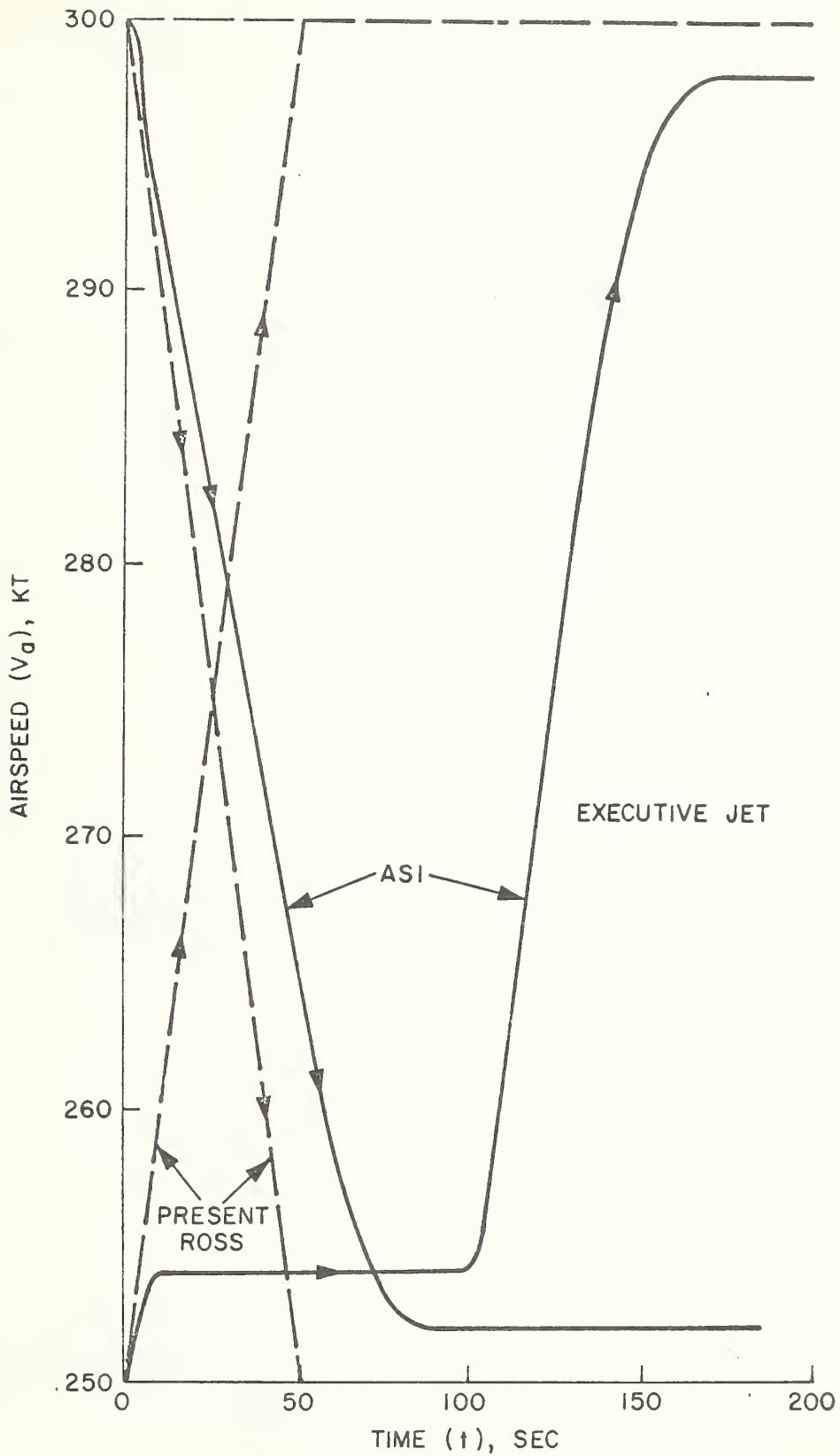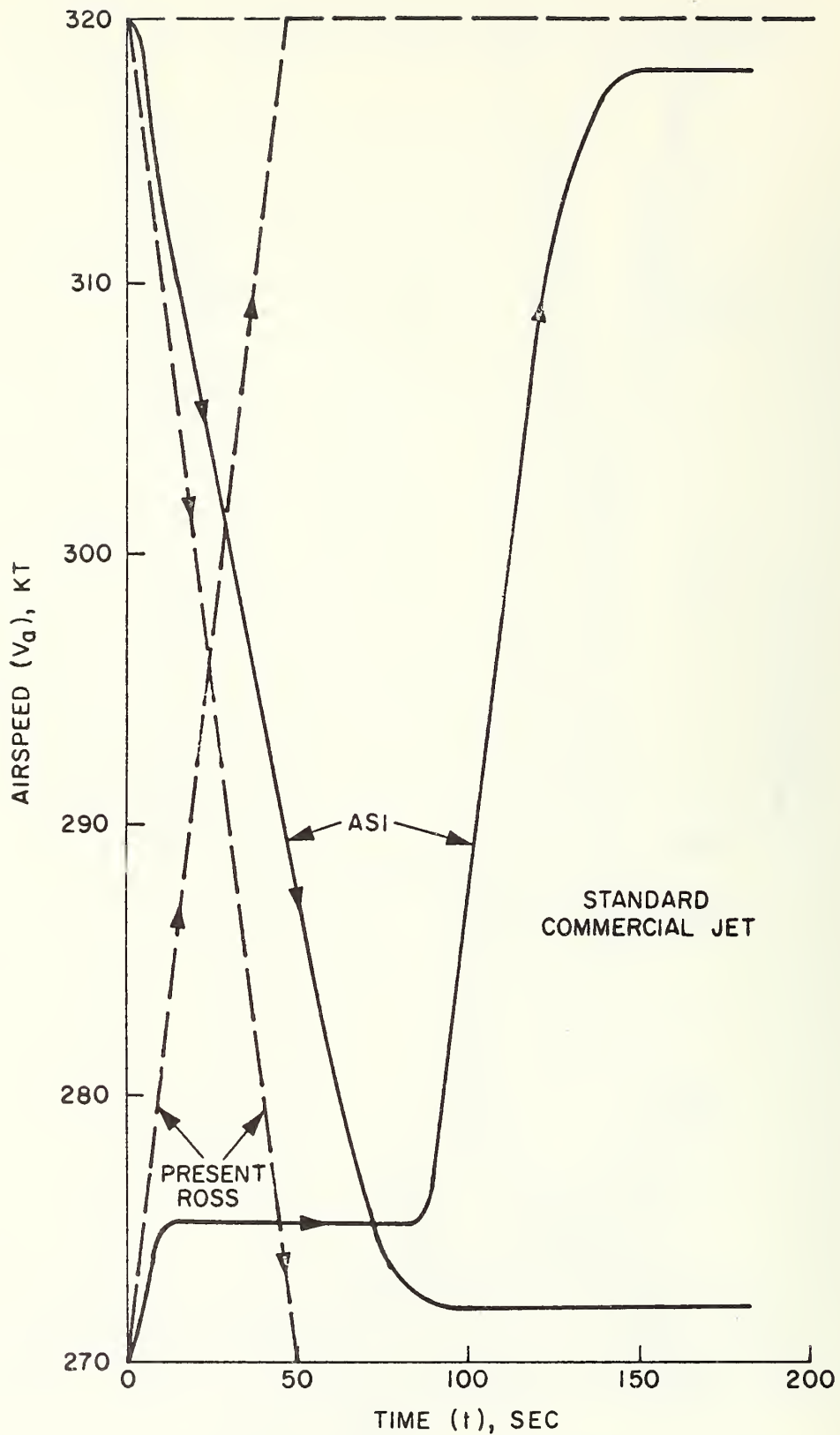
Figure 31. Comparison of ROSS and ASI Velocity Response Models
for Climbing Speed-Up and Descending Slow-Down
(Standard Commercial Jet Aircraft).

- 74 -

altitude response. However, in the revised model the altitude response limits

the acceleration or deceleration of the aircraft. In the slowing-down, descending

cases, the limit is not as effective since the normal rate of descent is somewhat

less than the maximum (see Table 1).

Heading changes also occur at constant rate in the present program.

The more sophisticated model allows a time lag for establishing the turn plus a

simulation of the pilot's turn logic which may cause slight over or under shoot

of the desired heading. The more sophisticated model would be desirable where

turn maneuvers are used for CAS or IPC, and also where path stretching is used

for separation, spacing or merging. The two model's responses are compared in

Figures 32 - 34 for heading changes of 10°, 30° and 90° respectively. The simulation

results in Figures 32 - 34 are for constant altitude and airspeed, and neglect any

air data system errors. The simulation was terminated when the heading was

within 0.5^{o} of the commanded value and the turn rate was less than 0.1 $^{o}/sec$.

Aircraft guidance along a desired track in the present simulation is

assumed to be perfect after the aircraft actual position is within 1.5^{o} of the desired

bearing. The new model for guidance along a desired track is much more sophisticated.

It uses a steering algorithm which depends on the distance off track and the heading

relative to the desired track angle. In order to acquire the track the aircraft is

first placed on an intercept heading of approximately 90° to the desired course.

Then when sufficiently close, the algorithm is changed to that of a linear, second-

order regulator which causes the aircraft to acquire the track with a slight overshoot.

Steady-state offset can occur because of a crosswind. The logic is similar to what

is used in coupled automatic pilots. The more sophisticated model would be preferred

whenever the acquisition of an assigned track is left to the pilot or whenever the

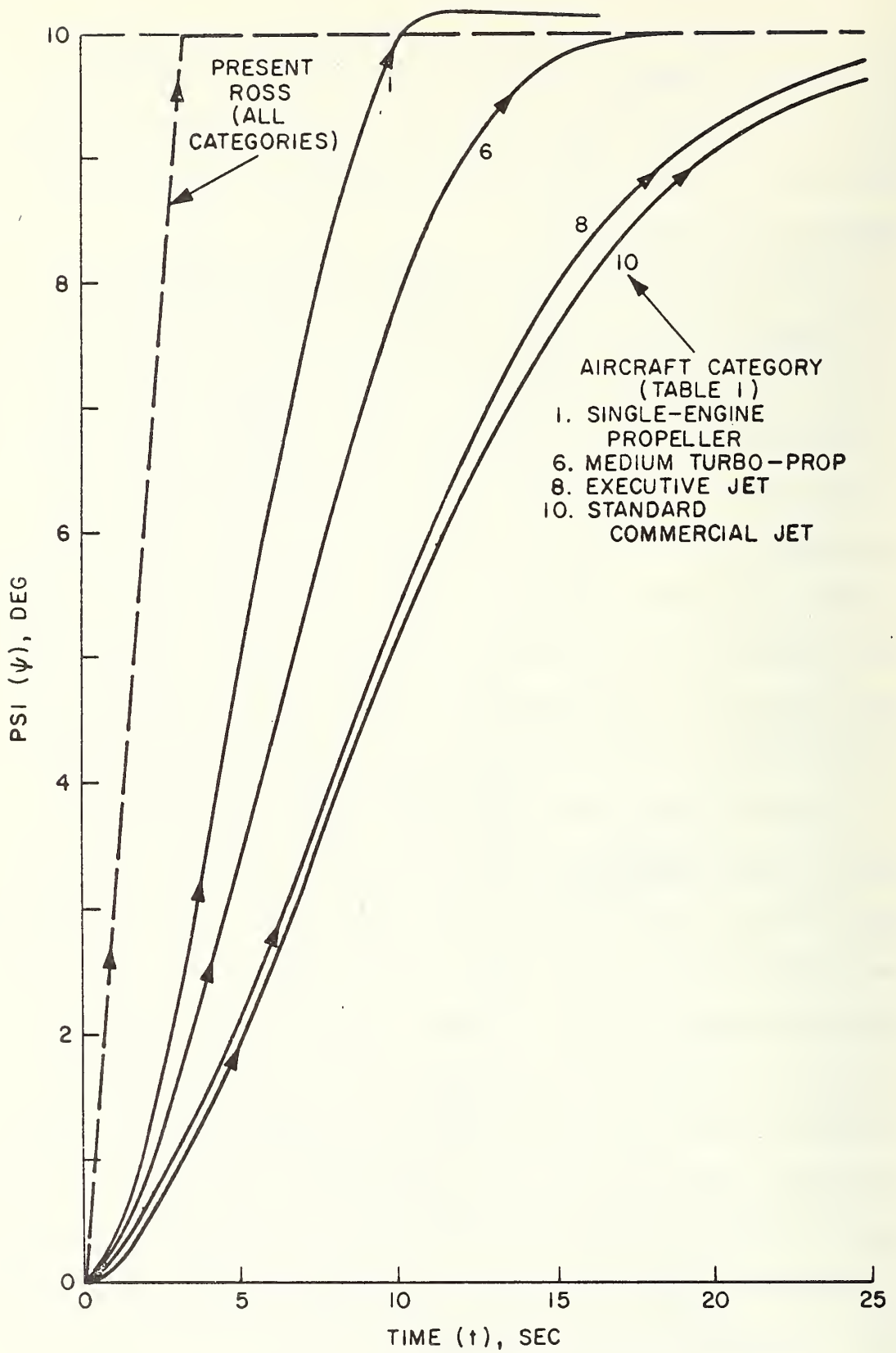tracking dynamics are of importance such as with closely spaced parallel track

Figure 32. Comparison of ROSS and ASI Heading Response Models for Various Aircraft Categories (10° Heading Change).
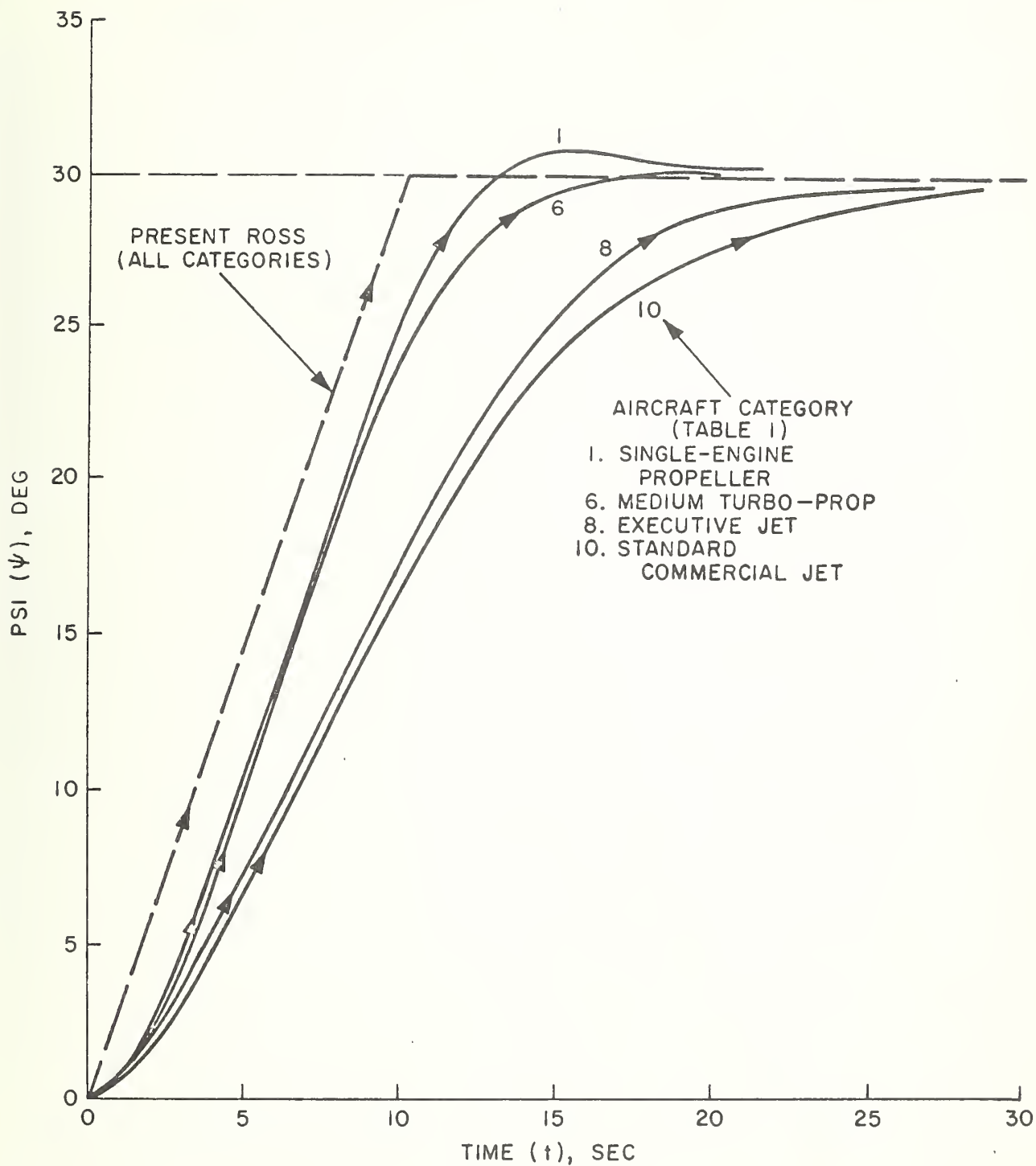
Figure 33. Comparison of ROSS and ASI Heading Response Models
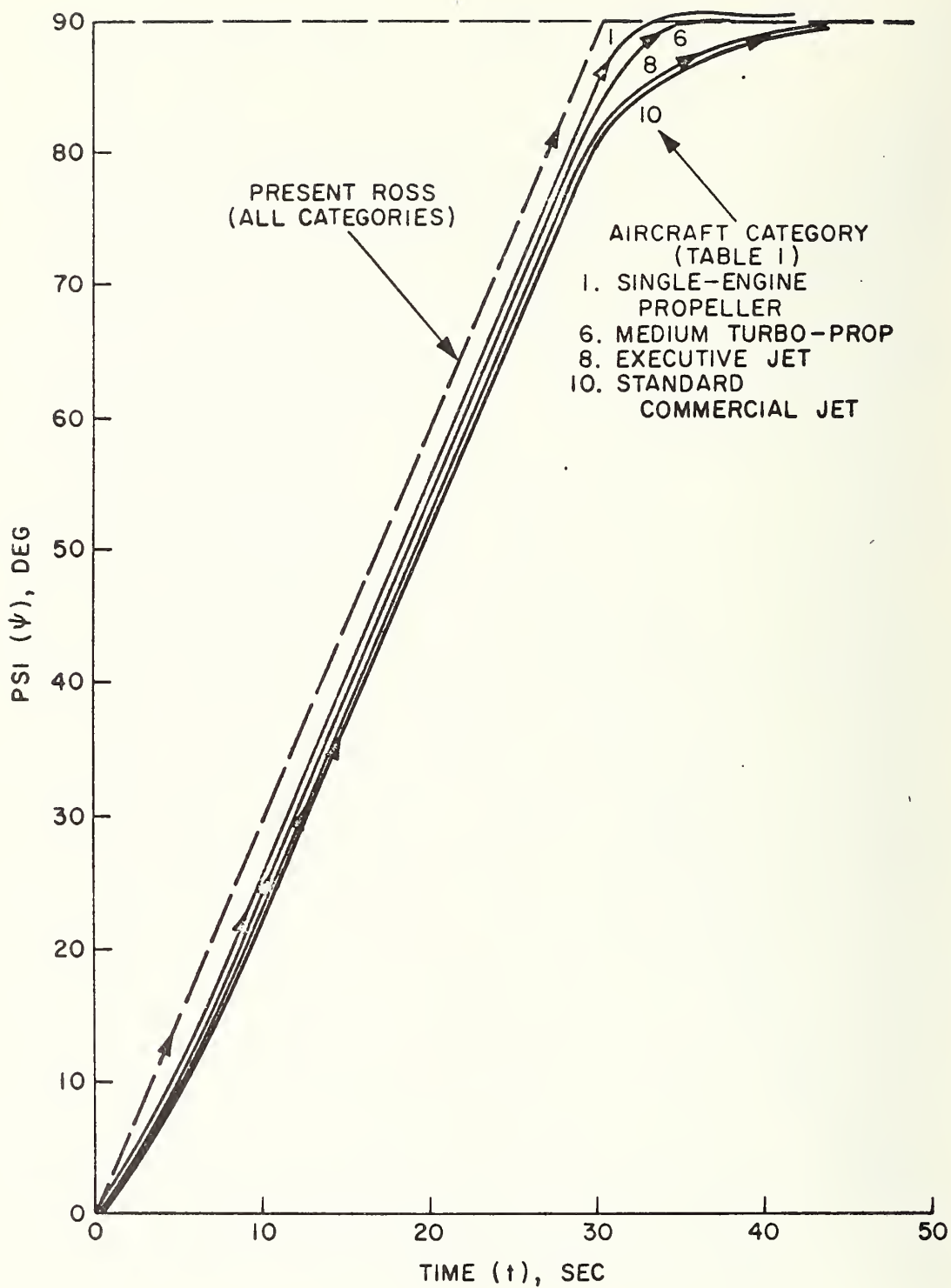for Various Aircraft Categories (30° Heading Change).

Figure 34. Comparison of ROSS and ASI Heading Response Models
for Various Aircraft Categories (90° Heading Change).

airways or ILS installation.

The navigation error in the present program consists of correlated noise added to the true cartesian position coordinates. Both components of position noise use the same standard derivation and correlation time. Navigation errors in the new models are more representative of specific navigation systems which might be in use. Various error sources can be identified to ascertain relative importance of errors. Geometric, computation and propagation errors can be changed independently. The more sophisticated model would be desirable when the objective of the experiment is to ascertain the relative importance of different types of error sources, or to evaluate competing navigation systems for particular applications.

The present surveillance error is computed by random selection of separate range and bearing bias errors defined by mean and standard deviation input values. The new model changes the range and bearing errors on each discrete scan and processes the radar data using the same basic tracking algorithms used in the third-generation system. The more sophisticated model should be used whenever the radar data is to be processed for velocity determination, conflict prediction, radar mosaics, etc.

It should be clear that the more sophisticated models can be used selectively, one at a time, depending upon the specific need. They might be applied only to one or two aircraft in a simulation or they can be invoked only when two aircraft are in a conflict situation. Used in this manner, the program is longer, but the increase in running time can be kept minimal. Experience with the program should show when the more sophisticated models are justified and when their increased realism is superfluous.

In summary, Table 4 presents a comparison of the present and revised models for the more important ATC system functional error sources. As indicated, the effects of certain of the lesser important or indescribable error sources have not yet been included in either model.

Table 4. Comparison of ATC System Functional Error Models.

FUNCTIONAL ERROR SOURCE	STANDARD ROSS MODEL	REVISED ASI MODEL
AIR DATA SYSTEM		
Altimeter	random bias*	bias a function of h
Rate of climb	random bias*	bias proportional to $\dot{h}$
Heading	random bias*	random bias
Airspeed/Mach No.	random bias*	bias proportional to V
NAVIGATION SYSTEM		
VOR	correlated noise in cartesian coordinates – no directivity	geometry, propagation, site & receiver errors modeled
DME		geometry, propagation, site & receiver errors modeled
RNAV	can be approximated as perceived x and y location errors relative to a described location	computed from VOR/DME errors
ILS	not modeled	not modeled
AIRCRAFT DYNAMICS		
Acceleration	no limits* instantaneous	limited by $\dot{h}$ first order lag
Climb rate	single rate* instantaneous	variable rate first order lag

*The description given applies to "standard" use of the simulator. At his option, the user can prepare route procedures that achieve other conditions. For example the bias of a value can be made proportional to the value, one rate can be made a function of another, etc.

Table 4. (Cont.)

FUNCTIONAL ERROR SOURCE	STANDARD ROSS MODEL	REVISED ASI MODEL
AIRCRAFT DYNAMICS (Cont.)		
Turn rate	single rate* instantaneous	variable rate lag for roll-in
Tracking	acquisition threshold no tracking error	complete acquisition dynamics 2nd order linear tracker
Pilot reaction time	not modeled	included in lags
Blunders	not modeled	not modeled
SURVEILLANCE SYSTEM		
Range error	fixed bias	random bias each scan
Azimuth error	fixed bias	random bias each scan
Geometry error	not included	included
Tracking algorithm	not included	simulated actual algorithm
WIND		
Variation with altitude	steady-state only	proper aircraft response
Variation with location	none	proper aircraft response
Prediction error	not modeled	not modeled

*
The description given applies to "standard" use of the simulator. At his option, the user can prepare route procedures that achieve other conditions. For example the bias of a value can be made proportional to the value, one rate can be made a function of another, etc.

Table 4. (Cont.)

FUNCTIONAL ERROR SOURCE	STANDARD ROSS MODEL	REVISED ASI MODEL
COMMUNICATIONS		
Delay	not modeled	not modeled
Garble	not modeled	not modeled
CONTROLLER		
Reaction time	not modeled	not modeled
Decision delay	not modeled	not modeled
Blunders	not modeled	not modeled

SECTION 8

CONCLUSIONS AND RECOMMENDATIONS

This section presents a summary of the important conclusions of the error analysis and modeling study, along with some suggested applications for the revised error models and possible additional improvements for the simulation.

8.1 SUMMARY OF CONCLUSIONS

The important functional error sources for the present and near-future ATC system were identified and analyzed for their relative effects on system performance. Error models were developed for the dominant functional error sources having response times of the order of three seconds or greater. The new models thus provide approximately an order of magnitude improvement for the ATC simulation over the existing models which generally neglect responses of less than about 30 seconds.

The new models provide the simulation user with the capability of experimenting with a number of future ATC system concepts which could not be properly evaluated with the present programs. Those ATC concepts which depend on higher frequency and more accurate responses can be effectively tested with confidence that the major error sources are included. Examples of the experiments which can be investigated with the new models include collision avoidance systems, intermittent positive control, 4-D navigation, and metering and spacing concepts.

The target dynamics models have been developed to duplicate as nearly as practicable the normal response that an actual pilot would produce. This required tradeoffs between computational complexity and realism. The models were constructed to be as independent of specific aircraft performance data as feasible.

As a result, the representation of a particular aircraft requires the specification of sixteen or fewer parameters and time constants. The altitude and airspeed/ heading control loops are uncoupled, except that the acceleration-deceleration capability is realistically limited during a simultaneous climb-descent.

The altitude, airspeed and heading control models contain nonlinear logic elements which required some verification of their intended operation. Simple check programs were developed, neglecting the air data system and wind effects, to evaluate the performance of these models. The results of the check programs conform to the desired response.

Analysis of the wind effects on system performance indicated that gusts will not be significant for the advanced ATC concepts mentioned previously. Consequently, gusts were neglected in the revised wind model. However, unknown steady-state winds and strong wind shears do appear to present problems, particularly for 4-D guidance and metering and spacing concepts.

The $\alpha - \beta$ tracker algorithm in the surveillance model introduces a significant delay in sensing groundspeed and can result in substantial errors in the estimated target position. The tracker was originally designed for the purpose of keeping the alphanumerics on the radar plan position indicator associated with the correct target; it was not intended to estimate groundspeed of the target. The $\alpha - \beta$ tracker is based on nonaccelerating flight, and consequently cannot accurately respond to rapid target maneuvers.

8.2   RECOMMENDED APPLICATIONS

Following are some recommended applications for the ATC simulation model. In most cases the experiments can be conducted with existing software and the newly-developed models presented in this report.

1.   Terminal Area Simulation - Error Assessment.

The purpose of this experiment is to examine the effects of wind, air data system errors, navigation errors and surveillance errors on safety, capacity, and control effort in the terminal area. The ATC simulation is exercised using a predetermined control process, while the relative contributions of the individual error sources are varied systematically. Safety is measured by the number of times a given separation criterion is violated. Capacity is defined by the number of aircraft handled per unit time. Control effort can be estimated by the number of control commands which are necessary.

2.   Enroute Area Simulation - Error Assessment.

The purpose of this experiment is to examine the effects of wind, air data system errors, navigation errors and surveillance errors on the accuracy of metering aircraft to the terminal area. The ATC simulation is programmed to feed aircraft to the terminal area landing process while each of the error sources is varied systematically. Metering accuracy is measured by the timing error at the terminal area input fix.

3.   4-D Guidance Simulation - Error Assessment.

The purpose of this experiment is to examine the effects of wind, air data system errors, navigation errors and surveillance errors on the ability of a target to follow a 4-D path. A typical arrival path must be established with arrival fixes designated along it. Then, a control logic for generating discrete commands to the aircraft must be developed. These commands should include both speed control and path stretching in order to correct for disturbances which change the arrival time. The accuracy of time of arrival will be measured in the face of wind, air data, navigation and surveillance system errors. Knowledge of an unsteady

wind is expected to be an important factor and the simulation should establish how accurately the wind should be known and to what granularity as a function of space and time.

4.   Inter-Aircraft Spacing Assessment.

A spacing and sequencing process which uses actual instead of planned information on the positions of targets may have efficiency and capacity advantages over fixed slot, preplanned processes. Previous applications have modeled the single aircraft when it is supplied a flight plan and position relative to navigational coordinates, but the important questions for the total system concern the inter-aircraft spacings. The strategy taken by both the controller and the individual aircraft commander must be modified in that each may now be influenced by the presence of additional aircraft. This requires development of a new sequencing and spacing algorithm, including the insertion of take-offs in gaps which open up in the landing flow.

Interactive simulation using human pilots and controllers is recommended first inasmuch as the existing system does not provide traffic information in the cockpit concerning nearby aircraft. Such a simulation does not need to be overly complex; each pilot needs only three controls to set velocity rate, heading rate and altitude rate. Aircraft dynamics and constraints described by the ASI models can be used to simulate various aircraft. The positions of all the simulated aircraft can be presented on a common display. After pilot strategy has been determined by observation it can be modeled for analytic simulation. The controller may be simulated by either a human or an analytic algorithm. Distributed tactical systems may be simulated by letting the human pilots operate without the controller in the loop. IPC systems may be simulated by modification of the strategy used by the controller and eliminating the pilot's access to the display. The first task

- 86 -

is to develop the interactive simulation. The second task is to observe the inter-actions and model the strategies used by both pilots and controllers under the various control concepts. The next task is to exercise the analytic models and compare the results to those obtained with human pilots and controllers. Finally, the analytic models can be exercised to evaluate the various control concepts. Capacity and risk evaluations can be determined from the inter-aircraft spacings which result.

5.   Separation Assurance Concepts Evaluation.

The ATC simulation can be applied to the evaluation of proposed CAS and IPC concepts. At present the traffic situation can be programmed so that targets fly prescribed tracks and respond to input commands. A number of new concepts and codings will have to be developed. First, a hazard criterion must be defined in terms of relative position, relative speed and relative acceleration. Algorithms must be established for checking collision pairs for violation of the hazard criterion, and for resolving the hazard and issuing appropriate commands to the aircraft involved. Also, the aircraft has to be returned to normal flight following the hazard resolution. Finally, coding must be provided for keeping statistics on true, false and missed alarms, duration of hazards, distance of closest approach, and other evaluation parameters.

REFERENCES

1.   Ricci, R. C. and Roy, J. R., "Multi-Modal Transportation System Simulation", Proceedings of the Summer Computer Simulation Conference, Boston, Massachusetts, July 19-21, 1971.

2.   Erwin, R. L., Jr., "Time-Synchronized Approach Control", Journal of the Institute of Navigation, Vol. 17, No. 3, Fall 1970.

3.   Hynes, R. J., Stevenson, L. E. and Capen, E. B., "4-D Guidance of STOL Aircraft", AIAA Paper No. 71-770, AIAA 3rd. Aircraft Design and Operations Meeting, Seattle, Washington, July 12-14, 1971.

4.   Kuprajanow, A., Liedman, S., and Warshow, M., "Preliminary Evaluation of Selected Air Traffic Control Concepts", The Civil Aviation Research and Development Policy Study, November 1970.

5.   Holt, J. M. and Marner, G. R., "Separation Theory in Air Traffic Control System Design", Proceedings of the IEEE, Vol. 58, No. 3, March 1970, pp. 369-376.

6.   Pogust, F. and Hooton, T., "Terminal Area Traffic Sequencing - Some Guidelines for Computer Design", 17th. Technical Conference, International Air Transport Association, Lucerne, Switzerland, October 1967.

7.   Simpson, R. W., "An Analytical Investigation of Air Traffic Operations in the Terminal Area", Massachusetts Institute of Technology, PhD. Thesis, May 15, 1964.

8.   Anon., "Computer-Aided Metering and Spacing with ARTS III, Phase I Design Study", Computer Systems Engineering, Inc., December 1970.

9.   Koenke, E. J., "A Theory of Aircraft Collision Avoidance System Design and Evaluation", Transportation Systems Center, Report No. DOT-TSC-OST-71-4, March 1971.

10.   Anon., "Report of Department of Transportation Air Traffic Control Advisory Committee", US Government Printing Office, December 1969.

11.   Anon., "ROSS Technical Manual", Bolt, Beranek and Newman, Inc., July 26, 1971.

12.   Anon., "The BBN Air Traffic System User Guide", Bolt, Beranek and Newman, Inc., 1971.

13.   Anon., "Instrument Flying Handbook", AC61-27B, US Government Printing Office, 1971.

14.   Kayton, M. and Fried, W. R., "Avionics Navigation Systems", John Wiley and Sons, Inc., 1969.

15.   Erzberger, H. and Lee, H. Q., "Optimum Hotizontal Guidance Techniques for Aircraft", Journal of Aircraft, Vol. 8, No. 2, February 1971, pp. 95-101.

16.   Anon., "Mark-2 Subsonic Air Data System", ARINC Characteristic No. 565, February 15, 1968.

17.   Cooper, R. A., "Barometric Altitude: the Problem, Solution and Design", ASME Paper 60-AV-43, 1960.

18.   Erickson, R. A., "Accuracy of In-Flight Computation of Altitude from Air Data Inputs", NAVWEPS Report No. 7784, NOTS TP 2271. US Naval Ordnance Test Station, China Lake, Calif., December 1961, 28 pp.

19.   Gracey, W., "Recent Developments in Pressure Altimetry", AIAA Journal of Aircraft, May - June 1965.

20.   Anon., "Height Measurement in Supersonic Aircraft", Journal of Institute of Navigation (England), Vol. 19, 1965.

21.   Anon., "Pressure Altimetry Systems", Society of Automotive Engineers, ARP-942, 1967.

22.   Anon., "Mark 3 Sub-Sonic Air Data System (Digital DADS)", ARINC Characteristic 575-3, July 15, 1971.

23.   Anderson, S. R., "VHF Omnirange Accuracy Improvements", IEEE Transactions on Aerospace and Navigational Electronics, Vol. ANE-12, No. 1, March 1965, pp. 26-35.

24.   Brandewie, D. M. and Winick, A. B., "VOR/DME System Improvements", Proceedings of the IEEE, Vol. 58, No. 3, March 1970, pp. 430-437.

25.   Cochran, M. V., "The Characteristics and Potential of VOR/DME Area Coverage Capability", IEEE Transactions on Aerospace and Navigational Electronics, Vol. ANE-12, No. 1, March 1965, pp. 83-88.

26.   Dodington, S. H., "Recent Improvements in Today's DME", IEEE Transactions on Aerospace and Navigational Electronics, Vol. ANE-12, No. 1, March 1965, pp. 60-67.

27.   Flint, R. B. and Hollm, E. R., "VOR Evolutionary System Improvements in the United States", IEEE Transactions on Aerospace and Navigational Electronics, Vol. ANE-12, No. 1, March 1965, pp. 46-55.

28.   Johansen, H., "A Survey of General Coverage Navaids for V/STOL Aircraft - A VOR/DME Error Model", Massachusetts Institute of Technology, NASA CR-1588, October 1969.

29. McKeel, P. D. and Craymer, L. G., "Calibration, Flight Inspection and Performance Assurance of VOR/DME/VORTAC Facilities", IEEE Transactions on Aerospace and Navigational Electronics, Vol. ANE-12, No. 1, March 1965, pp. 15-25.

30. Prichard, J. H., "The VOR/DME/TACAN System, Its Present State and Its Potential", IEEE Transactions on Aerospace and Navigational Electronics, Vol. ANE-12, No. 1, March 1965, pp. 6-10.

31. Anon., "Airborne VOR Receiver", ARINC Characteristic No. 579, Aeronautical Radio, Inc., June 22, 1970.

32. Crone, W. J. and Kramer, E. L., "Development of the Doppler VOR in Europe", IEEE Transactions on Aerospace and Navigational Electronics, Vol. ANE-12, No. 1, March 1965, pp. 36-40.

33. Hollm, E., et al., "Precision VOR - Volume I: Development and Flight Test Program", RD-67-58-I, Airborne Instruments Laboratory, August 1967.

34. Hemesath, N. B., "Optimum Complementation of VOR/DME with Air Data", Journal of Aircraft, Vol. 8, No. 6, June 1971.

35. Bryson, A. E., Jr. and Bobick, J. C., "Improved Navigation by Combining VOR/DME Information and Air Data", AIAA Paper No. 71-928, AIAA Guidance, Control and Flight Mechanics Conference, Hempstead, New York, August 16-18, 1971.

36. Anon., "Minimum Operational Characteristics - Airborne DME Systems", DO-141, RTCA Special Committee SC-116C, August 14, 1969.

37. Hirsch, C. J., "A TACAN-Compatible Accurate DME for Short Ranges", IEEE Transactions on Aerospace and Navigational Electronics, Vol. ANE-12, No. 1, March 1965, pp. 68-75.

38. Anon.., "Mark 3 Airborne Distance Measuring Equipment", ARINC Characteristic No. 568-3, June 1, 1971.

39. Anon., "Airman's Information Manual, Part I, Basic Flight Manual and ATC Procedures", US Government Printing Office, November 1971.

40. Dinerman, B. V., "An Evaluation of the VOR/DME Omnitrack 1A Area Navigation System", NA-69-29 (RD-69-30), NAFEC, June 1969.

41. Anon., "Air Traffic Control Service for Area Navigation Equipped Aircraft Operating in the United States National Airspace System", Department of Transportation, Federal Aviation Administration, 7110.18, February 27, 1970.

42. Anon., "Minimum Operational Characteristics - Airborne Area Navigation Systems", DO-140, RTCA Special Committee SC-116E, August 14, 1969.

43.   Beningfield, H. W., "Design and Operational Considerations for the Course
        Line Computer", SAE Paper 690345, SAE National Business Aircraft Meeting,
        Wichita, Kansas, March 26-28, 1969.

44.   Wohl, B., "Sperry's 3-D Area-Nav System", Airport World, Vol. 4, No. 4,
        April 1971, pp. 38-40.

45.   Anon., "Symposium on Area Navigation", sponsored by Federal Aviation
        Administration, Washington, D. C., January 24-25, 1972.

46.   Hollister, W. M. and Brayard, M. C., "Optimum Mixing of Inertial Navigator
        and Position Fix Data", Measurement Systems Laboratory, MIT, RE-62, August
        1969.

47.   Hemesath, N. B., Mayer, D. H. and Schweighofer, H. M., Complementing
        VOR/DME with INS - An Improved Navigation System", SAE Paper 690338,
        SAE National Business Aircraft Meeting, Wichita, Kansas, March 26-28,
        1969.

48.   Weinstein, S. M., "Beacon Target Processing for Air Traffic Control",
        Proceedings of the IEEE, Vol. 58, No. 3, March 1970, pp. 408-412.

49.   Renick, R. C., "An Improved ATC Radar Beacon System", Proceedings of
        the IEEE, Vol. 58, No. 3, March 1970, pp. 413-421.

50.   Shaw, N. K. and Simolunas, A. A., "System Capability of Air Traffic Control
        Radar Beacon System", Proceedings of the IEEE, Vol. 58, No. 3, March 1970,
        pp. 399-407.

51.   Sklansky, J., "Optimizing the Dynamic Parameters of a Track-While-Scan
        System", RCA Review, Vol. 18, No. 2, July 1957, pp. 163-185.

52.   Benedict, T. R. and Bordner, G. W., "Synthesis of an Optimal Set of Radar
        Track-While-Scan Smoothing Equations", IRE Transactions on Automatic
        Control, Vol. AC-7, No. 4, July 1962, pp. 27-32.

53.   Sokkappa, B. G., "On the Application of Modern Estimation Techniques
        to Air Traffic Control", AIAA Paper No. 71-926, AIAA Guidance, Control
        and Flight Mechanics Conference, Hempstead, New York, August 16-18,
        1971.

54.   Bonin, L. J., "Comparison of SAGE/Buic and Kalman Filters for Air Traffic
        Control", AIAA Paper No. 71-58, AIAA 9th. Aerospace Sciences Meeting,
        New York, New York, January 25-27, 1971.

55.   Fries, J. R., "Improvement of Automatic Landing Through the Use of a Space
        Diversity ILS Receiving System", IEEE Transactions on Aerospace and Electronic
        Systems, Vol. AES-7, No. 1, January 1971, pp. 47-53.

56.   Semmelhack, H. P. and Hoppe, S. G., "Modern Techniques for Automatic Track-While-Scan", Proceeding of Second Hawaii International Conference on System Sciences, Honolulu, Hawaii, January 22-24, 1969, pp. 431-434.

57.   Singer, R. A., "Estimating Optimal Tracking Filter Performance for Manned Maneuvering Targets", IEEE Transactions on Aerospace and Electronic Systems, Vol. AES-6, No. 4, July 1970, pp. 473-483.

58.   Anon., "ARTS III Coding Specifications for the Modular Automated Terminal Air Traffic Control System", PX6047, Univac Federal Systems Division, August 1970.

BIBLIOGRAPHY

Astholz, P. T., "Increasing Runway Capacity", Society of Automotive Engineers National Air Transportation Meeting, No. 700820, New York, New York, April 20-23, 1970.

Baker, B., "Avionics Enter a New Era", Rotor Wing, September 1971, pp. 23-27.

Barnsby, A. E. and Keenan, J. A., "Annotated Bibliography of Documents Related to Terminal Area Modeling", MITRE Technical Report, MTR-4070, March 11, 1969.

Benham, F., Hatch, A. and Kass, S., "Airspace Control Environment Simulator - System Description and Operating Procedure", Raytheon Company, Report No. DOT-TSC-131-1, August 5, 1971.

Blake, N. A. and Nelson, J. C., "A Projection of Future ATC Data Processing Requirements", Proceedings of the IEEE, Vol. 58, No. 3, March 1970, pp. 391-398.

Blumstein, A., "An Analytical Investigation of Airport Capacity", Cornell Aeronautical Laboratory, Inc., Report No. TA-1358-G-1, June 1960.

Burrows, J. W., "Combined Inertial-ILS Aircraft Navigation Systems", Journal of Aircraft, Vol. 8, No. 6, June 1971.

Bush, Dr. R. W., Blatt, H. and Brady, F. X., "An Airborne Traffic Situation Display System", AIAA Paper No. 71-929, AIAA Guidance, Control and Flight Mechanics Conference, Hempstead, New York, August 16-18, 1971.

Chapman, C., "Measurement and Analysis of Enroute ATC Digital Radar System Errors", Interim Report, July 1970 - March 1971, FAA-NA-71-16, September 1971.

Chilton, R. G., "Some Measurements of Atmospheric Turbulence Obtained From Flow-Direction Vanes Mounted on an Airplane", National Advisory Committee for Aeronautics, Technical Note 3313, November 1954.

Feyer, L. H. W. and Nattrodt, K., "Test Results from a Tower VOR over a Forest Area", IEEE Transactions on Aerospace and Navigational Electronics, Vol. ANE-12, No. 1, March 1965, pp. 41-45.

Gracey, W., "The Measurement of Pressure Altitude on Aircraft", National Advisory Committee for Aeronautics, Technical Note 4127, October 1957.

Gracey, W., Jewel, J. W., Jr. and Carpenter, G. T., "Measurement of the Errors of Service Altimeter Installations During Landing-Approach and Take-Off Operations", National Aeronautics and Space Administration, Technical Note D-463, November 1960.

Graham, D., Clement, W. F. and Hofmann, L. G., "Manual Control Theory Applied to Air Traffic Controller-Pilot Cooperation", Systems Technology, Inc., P-110.

Harris, R. H., "Models for Runway Capacity Analysis", MITRE Technical Report, MTR-4102, October 30, 1969.

Hawthorne, W. B. and Daugherty, L. C., "VOR/DME/TACAN Frequency Technology", IEEE Transactions on Aerospace and Navigational Electronics, Vol. ANE-12, No. 1, March 1965, pp. 11-14.

Hollister, W. M. and Bansal, D. D., "Guidance and Control for V/STOL Aircraft", Measurement Systems Laboratory, MIT, RE-77.

Huston, W. B., "Accuracy of Airspeed Measurements and Flight Calibration Procedures", National Advisory Committee for Aeronautics, Report No. 919, 1948.

Jackson, A. S., Morse, R. V. and Crocker, J. P., "A Fast-Time Simulation Model of Automated Terminal Area ATC Systems", Control Technology, Inc., November 1962.

Jackson, A. S., et al., "Terminal Area Sequencing and Control", The TRW Computers Co., Air Traffic Control Studies, Report No. 10, February 1961.

Keenan, J. A. and Barnsby, A. E., "Functional Description of Basic Terminal Approach Simulation Model", MITRE Technical Report, MTR-4071, March 21, 1969.

Klass, P. J., "Discrete Address Beacon Plan Set", Aviation Week and Space Technology, October 18, 1971.

Koetsch, J. F., "A Three Dimensional Mathematical Model of the Air Traffic Control Separation Problem", International Aviation Research and Development Symposium, Atlantic City, New Jersey, April 10-14, 1961.

Larson, T. J. and Webb, L. D., "Calibration and Comparisons of Pressure-Type Airspeed-Altitude Systems of the X-15 Airplane from Subsonic to High Supersonic Speeds", National Aeronautics and Space Administration, D-1724, February 1963.

Litchford, G. B., "Analysis of Cumulative Errors Associated with Category II and III Operations with Requirements for Additional Research", Litchford Systems, NASA CR-1188, 1968.

McFarland, R. H., "Experiments in the Determination of VOR Radial Stability", IEEE Transactions on Aerospace and Navigational Electronics, Vol. ANE-12, No. 1, March 1965, pp. 56-59.

McFarland, R. H., et al., "VOR Propagation and Stability Study", RD-66-92, Ohio University, November 1966.

Melvin, W. W., "Effects of Wind Shear on Approach with Associate Faults of Approach Couplers and Flight Directors", AIAA Paper No. 69-796, AIAA Aircraft Design and Operations Meeting, Los Angeles, California, July 14-16, 1969.

Odoni, A. R., "An Analytical Investigation of Air Traffic in the Vicinity of Terminal Areas", Operations Research Center, MIT, Technical Report No. 46, December 1969.

Ottoson, H. I., "An Investigation of the Expected Magnitude of Control Errors in the TASC I System Transition Area", The Thompson-Ramo-Wooldridge Products Co., Air Traffic Control Studies Report No. 5, June 1960.

Ottoson, H. I., "Sensitivity of a Terminal Area Control Concept to Uncertainties in Control Information", MITRE Technical Report, MTR-4076, March 19, 1969.

Panofsky, H. A., "A Review of the Distribution of Wind and Temperature in the Lower Stratosphere", IAS Paper No. 60-25, IAS 28th. Annual Meeting, New York, New York, January 25-27, 1960.

Rempfer, P. S., et al., "Fixed-Base Simulation Evaluation of Various Low-Visibility Landing Systems for Helicopters", NASA TN-D-5913, March 1971.

Rosenshine, M., "Effects of Communications Constraints on Air Traffic Control System Capabilities", State University of New York at Buffalo, PhD. Thesis, May 1966.

Shames, O., "A Method of High-Speed Search for DME and TACAN", IEEE Transactions on Aerospace and Navigational Electronics, Vol. ANE-12, No. 1, March 1965, pp. 76-82.

Simpson, R. W., "A General Theory for Air Traffic Control", Introductory Lecture Notes, 16.78, Massachusetts Institute of Technology, January 1971.

Singer, R. A., and Behnke, K. W., "Real-Time Tracking Filter Evaluation and Selection for Tactical Applications", IEEE Transactions on Aerospace and Electronics Systems, Vol. AES-7, No. 1, January 1971, pp. 100-110.

Smith, M., et al., "Human Factors Analysis of Voice Communications Practices in Air Traffic Control", Convair/Pomona, TM 339-84, June 1960.

Stepner, D. E. and Tyler, J. S., Jr., "The Computation of Position Errors for Air Traffic Control Surveillance Models", AIAA Paper No. 71-927, AIAA Guidance, Control and Flight Mechanics Conference, Hempstead, New York, August 16-18, 1971.

Warfield, J. N., "Corrective System for Minimizing TACAN-DME Spurious Radiation", IEEE Transactions on Aerospace and Navigational Electronics, Vol. ANE-12, No. 1, March 1965, pp. 89-90.

Wenglin, S., "Geometrical Dilution of Precision in a Range-Range-Altitude Navigation System", ESD-TR-70-59, Mitre Corporation, March 1970.

Anon., "Altimetry", RTCA Paper 215-58/DO-88, RTCA Special Committee SC-70, November 1, 1958 (Reprinted January 27, 1969).

Anon., "Airspace Model Description", National Aeronautics and Space Administration, Electronic Research Center, ERC Internal Note No. 68-ASO-4, December 16, 1968.

Anon., "AINS-70 Area Inertial Navigation System", Collins Radio Co., October 29, 1970.

Anon., "A New Guidance System for Approach and Landing", Radio Technical Commission for Aeronautics, Special Committee 117, Document No. DO-148, December 18, 1970.

Anon., "Wind Shear", FAA Aviation News, May 1971, page 3.